

# Proposal for a Full-Scale Prototype Single-Phase Liquid Argon Time Projection Chamber and Detector Beam Test at CERN

M. A. Leigui de Oliveira, C. A. Moura, and L. Paulucci

*ABC Federal University*

R. Raboanary, H. T. Rakotondramanana, and L. Rakotondravohitra

*Univ. of Antananarivo, Madagascar*

V. Singh

*Banaras Hindu University*

M. Weber

*Univ. of Bern*

D. Adams, M. Bishai, R. Brown, H. Chen, M. Diwan, J. Dolph,  
G. d. Geronimo, R. Gill, R. W. Hackenburg, J. Joshi, S. H. Kettell,  
B. Kirby, S. Li, Y. Li, G. Mahler, M. Mooney, W. Morse, Z. Parsa,  
M. Potekhin, X. Qian, V. Radeka, S. Rescia, R. Sharma, J. Stewart,  
C. Thorn, B. Viren, E. Worcester, M. Worcester, B. Yu, and C. Zhang

*Brookhaven National Lab.*

J. Bremer, U. Kose, D. Mladenov, M. Nessi, and F. Noto

*CERN, European Organization for Nuclear Research European Laboratory  
for Particle Physics*

S. Kohn and K.B. Luk

*Univ. of California Berkeley*

M. Smy and H. Sobel

*Univ. of California Irvine*

D. Cline, K. Lee, A. Renshaw, and H. Wang

*Univ. of California Los Angeles*

J. Marshall and M. Thomson

*Univ. of Cambridge*

E. Kemp

*Univ. de Campinas*

N. Buchanan, D. Cherdack, S-K. Lin, D. Warner, and R. J. Wilson

*Colorado State University*

J. Fowler and K. Scholberg

*Duke University*

M. Adamowski, C. O. Escobar, A. Himmel, E. James, M. Johnson,  
T. Junk, T. Kobilarcik, E. McCluskey, D. Montanari, B. Norris,  
R. Plunkett, B. Rebel, R. Rucinski, L. Sexton-Kennedy, T. Shaw,  
M. Stancari, J. Strait, G. Velez, and T. Yang

*Fermi National Accelerator Lab*

J. Maricic, R. Milincic, and Y. Sun

*Univ. of Hawaii*

A. Higuera and L. Whitehead

*Univ. of Houston*

B. Bhuyan

*Indian Institute of Technology Guwahati*

G. S. Davies, B. Howard, H. Merritt, M. Messier, S. Mufson, J. Musser,  
J. Urheim, and D. Whittington

*Indiana University*

A. Blake, D. Brailsford, J. Nowak, and P. Ratoff

*Lancaster University*

P. Calafiura, D. A. Dwyer, B. Fujikawa, V. M. Gehman, C. S. Lin,  
T. Loew, Y. Nakajima, S. Patton, H. M. Steiner, K.V. Tsang, and C. Tull

*Lawrence Berkeley National Lab.*

C. Andreopoulos, K. Mavrokoridis, and C. Touramanis

*Univ. of Liverpool*

L. Bartoszek, J. Boissevain, S. Elliott, G. Garvey, E. Guardincerri,  
T. Haines, D. Lee, Q. Liu, W. Louis, C. Mauger, G. Mills, J. Ramsey,  
K. Rielage, G. Sinnis, W. Sondheim, C. Taylor, R. Van de Water, and  
K. Yarritu

*Los Alamos National Laboratory*

J. Insler, T. Kutter, and M. Tzanov

*Louisiana State University*

J. Evans, J. Hewes, G. Karagiorgi, A. Szelc, and S. Söldner-Rembold

*Univ. of Manchester*

M. Marshak and G. Pawloski

*Univ. of Minnesota*

R. Gran and A. T. Habig

*Univ. of Minnesota (Duluth)*

D. Stefan and R. Sulej

*National Centre for Nuclear Research*

G. Barr and A. Weber

*Univ. of Oxford*

N. Barros, S. Grullon, P. Keener, J. Klein, K. Lande, M. Newcomer, and  
R. Van Berg

*Univ. of Pennsylvania*

N. Graf, D. Naples, and V. Paolone

*Univ. of Pittsburgh*

K.T. McDonald and W.R. Sands

*Princeton University*

M. Convery, B. Eberly, N.A. Graf, M. Graham, L. Rochester, Y. Tsai, and  
T. Usher

*SLAC National Acceleratory Laboratory*

C. Andreopoulos\* and A. Weber<sup>†</sup>

*STFC Rutherford Appleton Laboratory*

T. Gamble, V. A. Kudryavtsev, N. McConkey, N. J. Spooner, and  
L. F. Thompson

*Univ. of Sheffield*

J. Reichenbacher and J. Stock

*South Dakota School of Mines and Technology*

T. Coan and T. Liu

*Southern Methodist University*

C. K. Jung, X. Li, C. McGrew, G. Santucci, and Z. Vallari

*Stony Brook University*

T. Blackburn, J. Davies, L. Falk, J. Hartnell, S. Peeters, M. Tamsett, and  
B. Zamorano

*Univ. of Sussex*

A. Brandt, A. Chatterjee, K. De, A. Farbin, H. Hadavand,  
S. Shamsavarani, A. White, and J. Yu

*Univ. of Texas Arlington*

G. J. Barker, N. Grant, M. D. Haigh, and Y. A. Ramachers

*Univ. of Warwick*

M. Duvernois, L. Greenler, B. Paulos, D. Wahl, and D. Wenman

*Univ. of Wisconsin*

A. Ioannisian

*Yerevan Physics Institute*

C. Cantini, P. Crivelli, A. Gendotti, S. Murphy, C. Regenfus, A. Rubbia,  
F. Sergiampietri, T. Viant, and S. Wu

*ETH Zürich*

June 8, 2015

submitted on behalf of the DUNE collaboration

---

\*also Univ. of Liverpool

†also Univ. of Oxford

## Executive Summary

The Deep Underground Neutrino Experiment (DUNE) will use a large liquid argon (LAr) detector to measure the CP violating phase, determine the neutrino mass hierarchy and perform precision tests of the three-flavor paradigm in long-baseline neutrino oscillations. The detector will consist of four modules each with a fiducial mass of 10 kt of LAr and due to its unprecedented size will allow sensitive searches for proton decay and the detection and measurement of electron neutrinos from core collapse supernovae [1].

The first 10 kt module will use single-phase LAr detection technique and be itself modular in design. The successful manufacturing, installation and operation of several full-scale detector components in a suitable configuration represents a critical engineering milestone prior to the construction and operation of the first full 10 kt DUNE detector module at the SURF underground site. A charged particle beam test of a prototype detector will provide critical calibration measurements as well as invaluable data sets to quantify and reduce systematic uncertainties. These measurements are expected to ultimately improve the physics reach of the DUNE experiment. Comparably detailed information cannot be gained in-situ with the future DUNE detector at its underground location.

Following the positive response from the SPSC to our EoI [2] this proposal defines the detector parameters and outlines a beam measurement program necessary to achieve these critical DUNE milestones. We propose to construct and operate a single-phase LAr detector with an active (total) LAr detector mass of 400 t (700 t). The active LAr region measures 7.2 (width)  $\times$  7.0 (length)  $\times$  5.9 m<sup>3</sup> (height) on its sides. The detector components will be identical to what is currently foreseen for the first 10 kt DUNE detector module. The design incorporates the experience gained over many years of R&D, in particular it benefits in many aspects from the 35 t prototype detector at Fermilab [3, 4].

The beam should provide different types of negatively and positively charged primary particles with sub-GeV to several GeV in energy. The anticipated beam measurement program is expected to last several weeks and should ideally be conducted prior to the second long shutdown of the LHC in 2018.

The DUNE collaboration has identified the single-phase LAr prototype detector (DUNE-PT) and beam test at CERN as a logical and critically important next step towards its ultimate goal of building and running the DUNE experiment [1]. The anticipated proximity to and synergies with WA105 [5], which is developing a complementary LAr TPC technology which could be employed by DUNE in some far detector modules, enhances collaboration and is expected to foster community building. We plan to work towards a direct detector performance comparison of single and double phase LAr data in this well characterized test environment. A strong, experienced and growing team within the DUNE collaboration is in place to carry out the proposed activities.

# Contents

<b>1</b>	<b>Introduction</b>	<b>8</b>
1.1	Goals for the prototype detector and beam test . . . . .	8
1.2	Single-phase LAr detector . . . . .	10
<b>2</b>	<b>Scientific Motivation and Measurement Program</b>	<b>10</b>
2.1	Detector and beam requirements . . . . .	11
2.2	Beam particle requirements . . . . .	12
2.3	Detector physics validation tests . . . . .	14
2.4	Other measurements . . . . .	19
<b>3</b>	<b>Single-Phase LAr Detector</b>	<b>20</b>
3.1	DUNE detector plans . . . . .	20
3.2	DUNE-PT . . . . .	22
<b>4</b>	<b>Cryostat and Cryogenics System</b>	<b>34</b>
4.1	Cryostat . . . . .	34
4.2	Cryogenic system . . . . .	40
<b>5</b>	<b>Calibration</b>	<b>43</b>
<b>6</b>	<b>Charged Particle Test Beam Requirements</b>	<b>45</b>
6.1	Particle beam requirements . . . . .	45
6.2	EHN1 H4ext beamline and beam instrumentation . . . . .	45
6.3	Beam rates and run plan . . . . .	47
<b>7</b>	<b>Computing, Data Handling and Software</b>	<b>49</b>
7.1	Event size estimate and data volume . . . . .	50
7.2	Databases . . . . .	51
7.3	Computing and software . . . . .	51
<b>8</b>	<b>Installation and Infrastructure</b>	<b>53</b>
8.1	Installation . . . . .	53
8.2	Infrastructure . . . . .	54
<b>9</b>	<b>Schedule, Organization and Cost Estimate</b>	<b>55</b>
9.1	Organization . . . . .	55
9.2	Schedule . . . . .	57
9.3	Institutional Responsibilities . . . . .	57
9.4	Cost estimate and funding sources . . . . .	59
<b>10</b>	<b>Summary</b>	<b>60</b>

# 1 Introduction

*This document describes the motivation and technical details of the proposed prototype detector and beam test. In Section 1 we give a brief overview of the goals for the detector and beam test. Section 2 describes the scientific motivation and the planned program of measurements. The layout of the single phase liquid argon detector and technical details of the detector components are specified in Section 3. In Section 4 we provide information on the proposed cryostat which houses the detector as well as on the required cryogenics system. Section 5 introduces our approach to calibrating the detector and the necessary tools to do so. We describe the requirements for the charged particle beam and a preliminary run plan in Section 6. In Section 7 we estimate computing and data handling needs before we describe the installation procedure for the detector and the interface to the CERN Neutrino Platform in Section 8. We present schedule and organization for the proposed activities in Section 9 before we conclude in Section 10.*

## 1.1 Goals for the prototype detector and beam test

The CERN single-phase liquid argon prototype detector at CERN (DUNE-PT) is a crucial milestone for the DUNE experiment that will inform the construction and operation of the first 10 kt DUNE far detector module. The prototype detector and beam test serve two principal functions.

The first goal is to serve as an engineering prototype to validate the performance of all detector components, establish and commission detector production sites and associated quality assurance procedures and to validate the installation procedure.

The second goal is to measure and study the response of the detector to charged particles of different types and energies. Results from these measurements serve to assess systematic detector uncertainties and validate MC simulations. They also enable validation and tuning of event reconstruction algorithms and particle identification tools.

In order to mitigate the risks associated with extrapolating from a detector with a few TPC modules to one which contains several hundred it is essential to benchmark the operation of full-scale detector elements and perform measurements in a well characterized charged particle beam.

Numerous basic detector performance parameters can be established with cosmic ray muons and these results are a critical input to finalizing the production procedures of the first 10 kt DUNE far detector components. Potentially problematic components can be identified and improvements and optimizations of the detector design for future far detector modules can be developed. In particular, the following checks are anticipated:

1. characterizing the performance of full-scale TPC module
2. studying the performance of the photon detection system
3. testing and evaluating the performance of detector calibration tools
4. verifying the functionality of cold TPC electronics under LAr cryogenic conditions
5. performing a full-scale structural test under LAr cryogenic conditions

6. verifying argon contamination levels and associated mitigation procedures
7. developing and testing installation procedures for full-scale detector components
8. identifying flaws and inefficiencies in the manufacturing process

Experience gained from construction, installation and commissioning of DUNE-PT as well as performance tests with cosmic ray data are expected to lead to a detector optimization of equivalent phases for the DUNE far detector.

The use of a well-defined charged particle test beam will significantly enhance our understanding of the detector performance beyond the criteria already mentioned. The beam measurements will serve as a calibration data set to tune the Monte Carlo simulations and serve as a reference data set for measurements of the future DUNE detector. In order to make such precise measurements, the detector will need to accurately identify and measure the energy of the particles produced in the neutrino interaction with argon which will range from hundreds of MeV to several GeV. More specifically, the goals of the prototype detector and beam test measurements include the use of a charged particle beam to:

1. measure the detector calorimetric response for
  - (a) hadronic particles
  - (b) electromagnetic showers
2. study  $e/\gamma$ -separation capabilities
3. measure event reconstruction efficiencies as a function of energy and particle type
4. measure performance of particle identification algorithms as function of energy
5. assess single particle track calibration and reconstruction
6. validate accuracy of Monte Carlo simulations for relevant energy ranges as well as directions with respect to the wire-plane geometry
7. study other topics with the collected data sets
  - (a) pion interaction kinematics and cross sections
  - (b) kaon interaction cross section to remove proton decay backgrounds
  - (c) muon capture for charge identification

The CERN charged particle beam lines provide an opportunity to perform this crucial test of the proposed single-phase LAr TPC.

## 1.2 Single-phase LAr detector

The basic components of the liquid argon detector include a Time Projection Chamber (TPC) housed in a cryostat which is connected to a cryogenics system. The cryostat contains the liquid argon target material and the cryogenic system keeps the liquid argon at a temperature of 89K, and maintains the required purity through a pump and filter system. A 500 V/m uniform electric field is created within the TPC volume between cathode planes and anode wire planes. Charged particles passing through the TPC release ionization electrons that drift to the anode wires. The bias voltage is set on the anode plane wires so that ionization electrons drift between the first several (induction) planes and are collected on the last (collection) plane. Readout electronics amplify and continuously digitize the induced waveforms on the sense wires at several MHz, and transmit these data to the DAQ system for analysis. The wire planes are oriented at different angles allowing a 3D reconstruction of the particle trajectories in two dimensions, and the third dimension is provided by measuring the drift time. In addition to these basic components, a photon detection system is included in the design to provide timing information for events not associated with the neutrino beam, enabling the study of proton decay and be more sensitive to galactic supernova neutrinos. The photon detection system will also provide timing information for cosmics which are important for calibration purposes.

Our LAr detector design is characterized by a modular approach in which the LAr volume in the cryostat is instrumented with a number of identical Anode wire Plane Assemblies (APA) and associated Cathode Plane Assemblies (CPA). To a large extent, scaling from detector volumes containing a few of such modules to several hundred should be feasible with low and predictable risk.

## 2 Scientific Motivation and Measurement Program

The primary goals of DUNE are to constrain or discover CP violation in the lepton sector by determining the value of the CP violating phase,  $\delta_{CP}$ , and to determine the mass ordering of the three neutrino mass eigenstates. This will be accomplished through measurement of the appearance rate of electron neutrinos and electron anti-neutrinos as well as the corresponding disappearance rate of muon neutrinos and muon anti-neutrinos over the 1300 km baseline of the experiment. Other important physics goals include sensitive searches for proton decay (PD) and detection of supernova neutrinos.

The full power of the DUNE experiment to perform a careful test of the three-flavor paradigm will come from a measurement of the detected neutrino spectral shape over a broad energy range. For a baseline of 1300 km the first maximum of the oscillation probability occurs around 2 GeV and the second oscillation maximum is around 0.6 GeV, so the high intensity neutrino flux must be maximized in the energy range from 0.5 - 5 GeV. It is desirable to have sufficient flux in the sub-GeV energy range to enable a measurement of the rapidly changing spectral shape in the region of the second maximum in the oscillation probability. It is this requirement on the neutrino energy spectrum, and the subsequent energy range of charged particles that result from their interactions, that determines the performance requirements for the DUNE detectors.

One of the main goals of DUNE-PT test beam program is to perform measurements needed to control and understand systematic uncertainties in DUNE oscillation measurements. As an example of the importance of controlling detector related uncertainties, Fig. 1 shows the effect of a reconstructed neutrino energy scale shift of -5% on the measured appearance signal and backgrounds in DUNE. The expected signal shape is shown for several values of  $\delta_{CP}$ . Energy scale uncertainties will distort and shift the  $\nu_e$  appearance spectra and can mimic a non-zero  $\delta_{CP}$  phase.

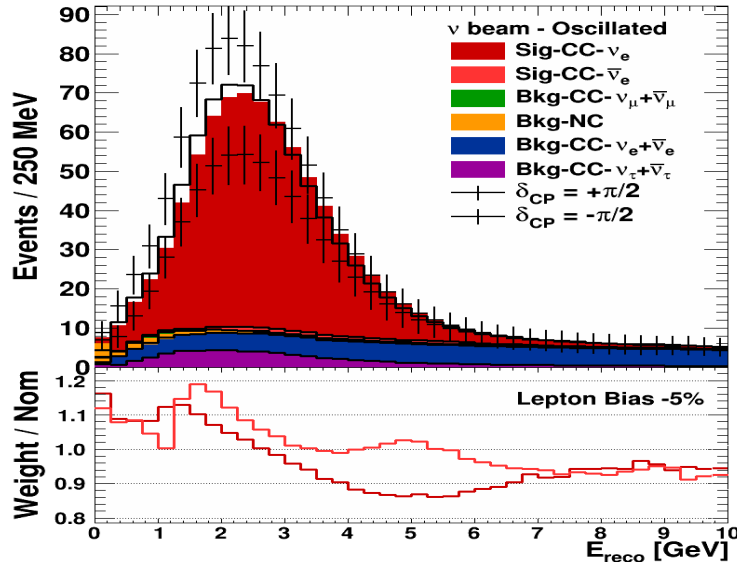


Figure 1: DUNE  $\nu_e$  appearance signal and background spectra. Solid curves show the effect of -5% reconstructed neutrino energy scale shift on the measured appearance  $\nu_e$  and  $\bar{\nu}_e$  signals assuming  $\delta_{CP} = 0$ . The crosses show the expected signal shape for  $\delta_{CP} = +\pi/2$  (lower crosses) and  $-\pi/2$  (upper crosses). Ratios show the distortion on the  $\nu_e$  and  $\bar{\nu}_e$  spectra due to the 5% energy scale shift.

Fig. 2 taken from [1] demonstrates that energy scale uncertainties will impact DUNE mass hierarchy (left) and  $\delta_{CP}$  (right) sensitivities. Work to evaluate the effect of all systematic uncertainties in DUNE sensitivities is still in progress. This study already indicates a significant reduction of the CPV peak sensitivity due to a reconstructed neutrino energy scale uncertainty. This example assumes linear neutrino energy scale variations at the levels indicated. More complex (and more likely) scenarios for energy scale uncertainties are under study and will likely result in larger effects on the sensitivities.

## 2.1 Detector and beam requirements

LAr TPC technology was first proposed for use in neutrino experiments by C. Rubbia in 1977 [6] but extensive use in neutrino experiments is only now being realized. The ICARUS T600 detector [7] pioneered the first large-scale detector when it operated in the CNGS neutrino beam at mean energy of  $\sim 17$  GeV. ArgoNeuT [8] [9] recently studied neutrino interactions in the NuMI beam down to sub-GeV energies with a small-scale (175 L fiducial volume) detector. While these samples are proving useful, they

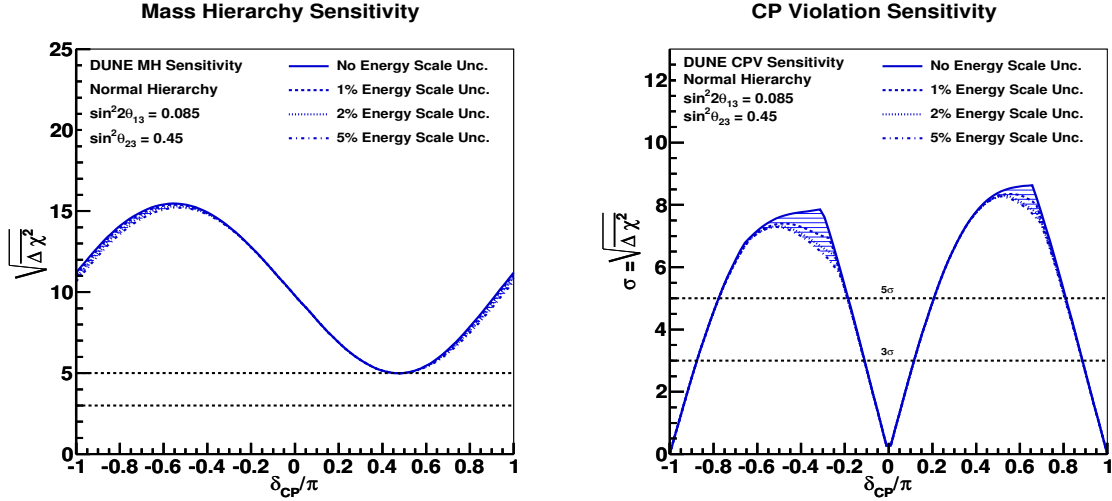


Figure 2: One scenario for the effect of 1-sigma neutrino energy scale uncertainties on DUNE projected sensitivity for mass hierarchy (left) and  $\delta_{CP}$  (right). In the left figure, the beam conditions are chosen so that the case with no energy scale systematic provides a significance of at least  $5\sigma$  for all values of  $\delta_{CP}$ . In the right figure, the beam conditions are chosen so that the case with no energy scale systematic provides a significance of at least  $3\sigma$  for 75% of  $\delta_{CP}$  values. Sensitivities are for true normal hierarchy; neutrino mass hierarchy and  $\theta_{23}$  octant are assumed to be unknown.

do not allow full isolation of the low energy neutrino interaction processes and final states from reconstruction and detector effects. The use of this technology in future precision neutrino experiments will require dedicated information on particle response in the sub-GeV to few-GeV range provided by charged-particle test beams.

The DUNE experiment will run in both neutrino and anti-neutrino configurations. These beams will be composed mainly of muon neutrinos (anti-neutrinos) as well as electron neutrinos (anti-neutrinos). In Fig. 3 the distributions of momenta and angles of particles created in neutrino interactions from simulated beam fluxes, including oscillation effects, are shown. The particle rates are normalized to the number of neutrino interactions in the DUNE far detector and to the neutrino beam flux.

DUNE-PT is designed from components that match exactly the DUNE far detector reference design for the first 10 kt detector module. The test beam detector must be sufficiently large in both longitudinal and transverse dimensions to contain showering particles up to the energy range of interest ( $\sim 10$  GeV). Fig. 4 shows the simulated longitudinal and transverse energy containment for proton showers up to 10 GeV in energy. For 10 GeV showers, more than 95% of the energy is contained in a detector of longitudinal size of 6 m and radius of 2.5 m. Showers from pions, kaons, and electrons have also been studied and similar or better containment is achieved in those cases, given the above detector dimensions.

## 2.2 Beam particle requirements

Table 1 summarizes the requested particle types and momenta along with required sample sizes for the test beam program.

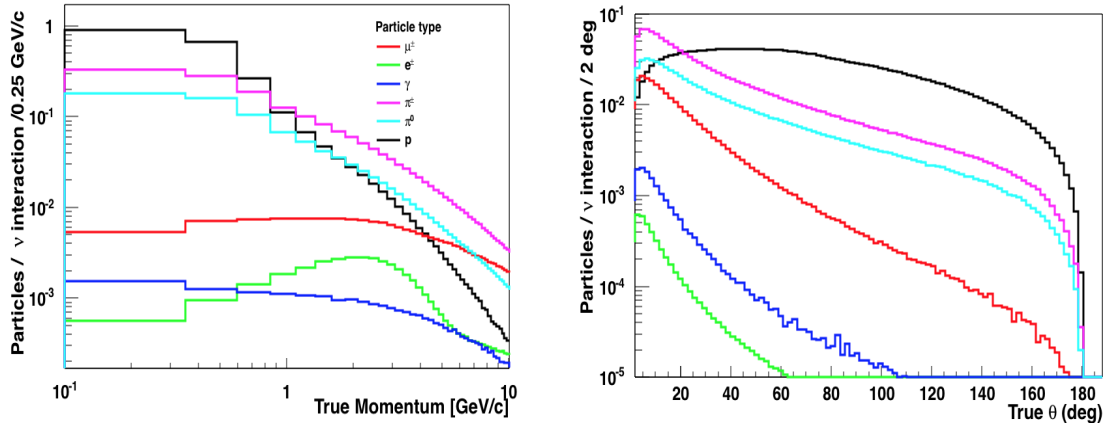


Figure 3: Particle momenta (left) and angular (right) distributions for particles produced in neutrino interactions from  $\nu_e$ ,  $\nu_\mu$ ,  $\bar{\nu}_e$  and  $\bar{\nu}_\mu$  from the neutrino mode of the beam and at the far detector location.

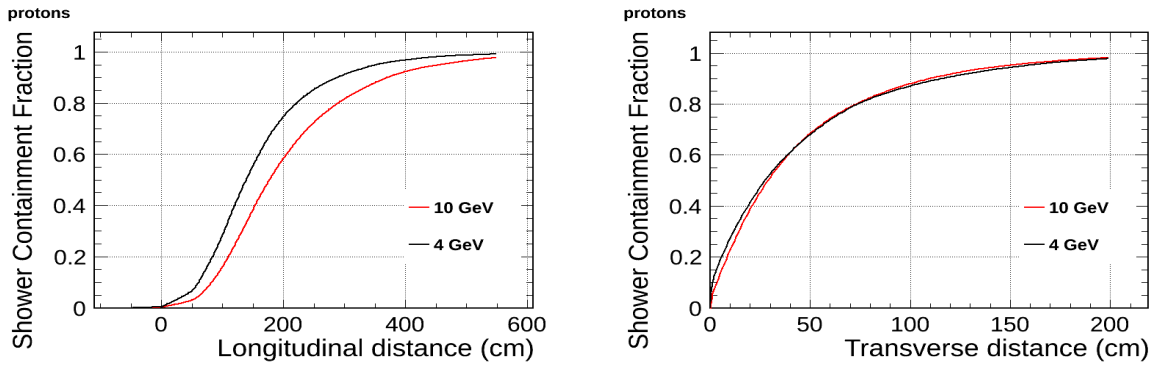


Figure 4: Simulated longitudinal and transverse containment for proton showers of 4 and 10 GeV/c momenta.

Pions and protons spanning the energy range expected in DUNE beam neutrino interactions will be used primarily to study hadronic shower reconstruction and calibration as described in Sec. 2.3.1 as well as particle identification (PID) algorithms discussed in Sec. 2.3.4. A sample of 600k 2 GeV  $\pi^+$  will be used to study secondary  $\pi^0$  over a large angular range to tune and calibrate electron/photon separation algorithms (see Sec. 2.3.6). A large sample ( $10^6$ ) of 1 GeV protons represents a sample of low energy stopping protons over a wide angular range needed to study angular dependent effects on collected charge as described in Sec. 2.3.3. Electrons will be used to benchmark and tune electron/photon separation algorithms and to calibrate electromagnetic showers as discussed in Sec. 2.3.6. Muon (and anti-muon) samples are needed to study reconstruction and PID calibration. Associated samples of Michel electron events will be used to calibrate algorithms for charge-sign determination (see Secs. 2.3.5 and 2.4).

Charged-kaon samples will be useful to characterize kaon PID efficiency for proton decay sensitivity but may be hard to obtain. The anti-proton sample will be helpful for exotic physics sensitivity studies. Both of these lower priority requests are discussed in Sec. 2.4.

Particle	Momenta (GeV/c)	Sample Size	Purpose
$\pi^+$	0.2, 0.3, 0.4, 0.5, 0.7, 1, 2, 3, 5, 7	10k	hadronic cal, $\pi^0$ content
$\pi^-$	0.2, 0.3, 0.4, 0.5, 0.7, 1	10k	hadronic cal, $\pi^0$ content
$\pi^+$	2	600k	$\pi^0/\gamma$ sample
proton	0.7, 1, 2, 3	10k	response, PID
proton	1	1M	mis-ID, PD, recombination
$e^+$ or $e^-$	0.2, 0.3, 0.4, 0.5, 1, 2, 3, 5, 7	10k	$e-\gamma$ separation/EM shower
$\mu^-$	(0.2), 0.5, 1, 2	10k	$E_\mu$ , charge sign
$\mu^+$	(0.2), 0.5, 1, 2	10k	$E_\mu$ , Michel el., charge sign
$\mu^-$ or $\mu^+$	3, 5, 7	5k	$E_\mu$ MCS
anti-proton	low-energy tune	(100)	anti-proton stars
$K^+$	1	(13k)	response, PID, PD
$K^+$	0.5, 0.7	(5k)	response, PID, PD
$\mu$ , e, proton	1 (vary angle $\times 5$ )	10k	reconstruction

Table 1: Requirements summary for particle types and momenta. The sample size column indicates the number of particles for each momentum point. Items in parenthesis indicate lower priority (see text).

## 2.3 Detector physics validation tests

The measured energy deposition for various particles and its dependence on the direction of the particle will be used to tune Monte Carlo simulations and allow improvements to reconstruction of neutrino energy and interaction topologies. Measurements of the response to charged particles and photons with the DUNE-PT will extend and be complementary to measurements made with other smaller detectors, such as LArIAT [10] and CAPTAIN [11].

### 2.3.1 Shower calibration

Accurate measurement of neutrino energy will require reconstruction of both electromagnetic and hadronic showers. Reconstruction of hadron energy in these energy ranges will require knowledge of the fate (interact, decay, or stop) of the initiating hadron ( $\pi^{+/-}$ ,  $p$ , or  $K^{+/-}$ ). For the case of interacting hadrons the composition of secondaries will need to be determined to characterize the response. These will include neutrals and particles which deposit energy electromagnetically ( $\pi^0$ ,  $\gamma$ ), as well as secondary hadrons. The test beam with known incoming particle type and momentum will be used to characterize interacting hadrons in this energy range.

Fig. 5 shows the fraction of true energy deposited by interacting protons with 1 GeV/c (left) and 3 GeV/c (right) incident momenta simulated using FLUKA particle transport code [12]. Interacting protons (65% of the 1 GeV/c sample) are selected. For this study, visible energy is summed using hit information with corrections applied for the lifetime of the drift electrons (No attempt is made to correct for recombination effects or electromagnetic shower fractions). The resulting energy deposition in the two cases cannot be accurately characterized by an average shower calibration factor. Monte Carlo

simulations of outgoing particles, especially at low energies, must be checked and benchmarked against calibration data to avoid large uncertainties from shower modeling.

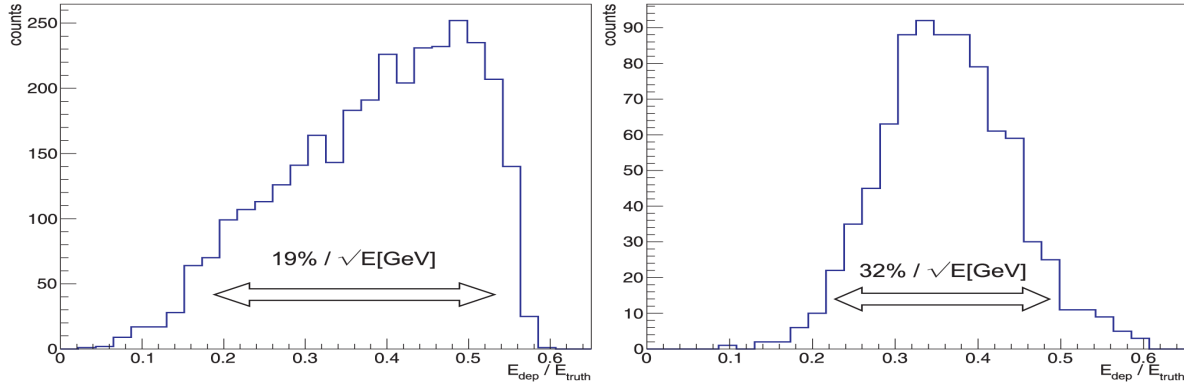


Figure 5: Fraction of true energy deposited by interacting protons of 1 GeV/c (left) and 3 GeV/c (right) momenta simulated using FLUKA [12].

Pion showers at low energies will also be important both for determining the interacted neutrino energy as well as for modeling neutral current backgrounds resulting from  $\pi^0$  content in showers. Significant differences in energy deposited in interactions initiated by  $\pi^+$  versus  $\pi^-$  are present up to momenta on the order of 1 GeV/c due to different final state particles and interaction cross sections. This is illustrated in Fig. 6 which shows the differences in mean energy deposited (left) and width (right) for interacting pions ranging from 0.2 GeV/c up to 5 GeV/c momenta. Resulting shower calibrations and reconstruction will differ and therefore each charge must be studied separately.

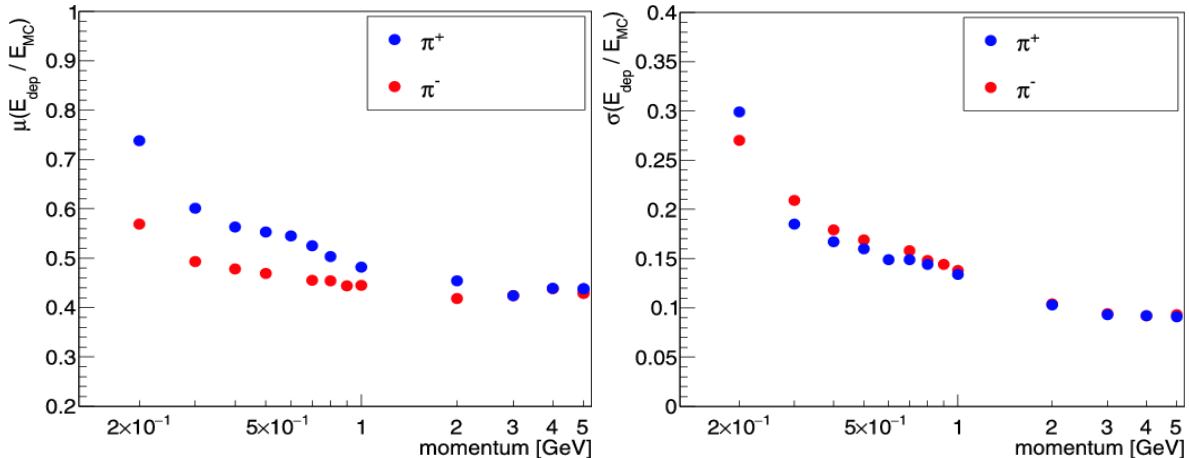


Figure 6: Differences in mean energy deposited (left) and width of visible energy (right) for interacting  $\pi^+$  versus  $\pi^-$  ranging from 0.2 GeV/c up to 5 GeV/c.

### 2.3.2 Cross section measurements

Final state pions are produced copiously in neutrino interactions in the energy range of interest and contribute substantially to total visible energy in the interaction. These

particles can re-interact either in the nuclear medium or after emerging from the target nucleus and substantially change the visible energy deposited in the event. The importance of modeling final state pion interactions on reconstructed neutrino energy have been recently demonstrated in the NuMI and Booster beam energy ranges [13,14].

Detailed knowledge of pion-nucleus cross sections in the sub-GeV energy range is required to tune generators [15] to accurately model event visible energy. Existing data used to tune the models cover limited energies (<200 MeV) and are primarily on lighter target nuclei [16]. The requested  $\pi^+$  and  $\pi^-$  samples will allow new data samples for measuring exclusive final state processes over the full relevant energy range and specifically on argon nuclei.

### 2.3.3 Angular dependence

An angular dependent track correction must be applied to deposited charge to accurately calibrate  $dE/dx$  that is used for track momentum and particle ID (see Sec. 2.3.4). An additional angular dependent effect could be present due to charge recombination. For example, Jaffe columnar recombination model [17,18] predicts angular dependence given by

$$Q \approx \frac{Q_o}{1 + k_c(dE/dx)/\mathcal{E} \sin \phi},$$

where  $Q_o$  and  $Q$  are the ionization charge and the collected charge respectively,  $k_c$  is a constant that depends on LAr diffusion and mobility coefficients,  $\mathcal{E}$  is the electric field strength, and  $\phi$  is the angle relative to the drift direction. ICARUS [19] and LArSoft default recombination models do not currently incorporate angular dependence. Recent results from ArgoNeuT [18] find a small unmodeled angular dependence in a data sample obtained using stopping protons from neutrino interactions in the range 50-300 MeV with angles in the range 40-90°.

Additional data covering a large angular range would be useful to further investigate angular dependence. The large sample of 1 GeV protons requested will also be used to study this using samples of secondary stopping protons produced in showers at a range of angles with respect to the field direction.

### 2.3.4 Bethe-Bloch parametrization of charged particles and PID

Information on range and charge deposition for stopping charged-particles can be used to accurately identify particle type as well as measure kinetic energy. Fig. 7 (left) shows track energy loss per unit length<sup>1</sup> ( $dQ/dx$ ) as a function of residual track range for simulated muon, pion, proton and kaon particle tracks. A neural-net-based algorithm [20,21] was used to determine PID functions for each particle hypothesis. Fig. 7 (right) shows the distribution of reconstructed  $dQ/dx$  in a narrow bin of residual range  $6(\pm 1)\text{cm}$  to illustrate the scale of difference between particle types. Proton and kaon bands are well separated from each other and from pion and muon bands, while pion and muon bands are almost overlapping which is challenging for the efficient separation. Simu-

---

<sup>1</sup>Signal attenuation due to recombination effect is not corrected for the PID purpose since it is a deterministic transformation which does not add measurement information.

lation is performed with FLUKA [12] and ICARUS geometry (3 mm wire pitch) and reconstruction code [22].

The PID efficiency and purity will depend on the detector configuration, geometry and reconstruction algorithm. The DUNE APA configuration and reconstruction algorithms may give significantly different results, especially for pion/muon separation. It is therefore important to test PID in a realistic prototype detector data in the presence of all detector effects. Event samples which include an adequate number of stopping particles for each species (muon, pions, protons and kaons) are included in the particle summary request in order to perform tests of PID algorithms and Bethe-Bloch calibration measurements.

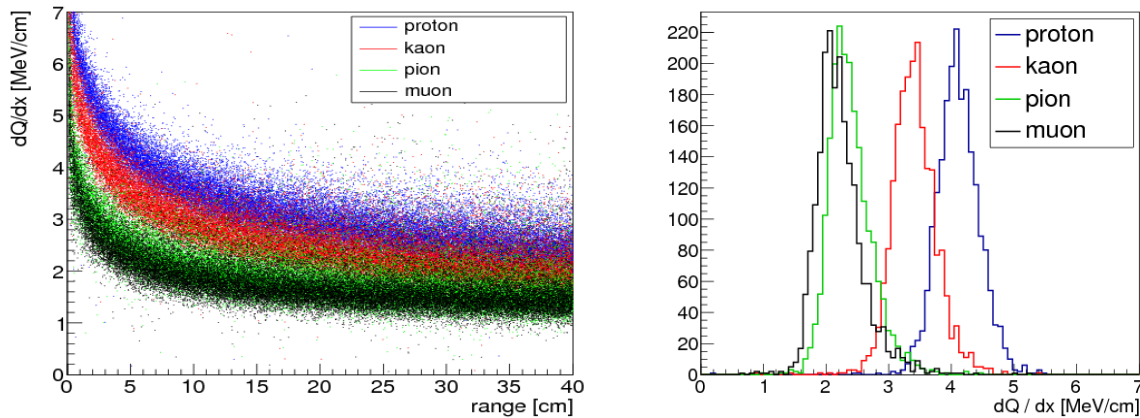


Figure 7: ICARUS simulated track  $dQ/dx$  as a function of residual range for muons, pions, protons and kaons, used as training data in a neutral-net-based PID algorithm (left). Distribution of  $dQ/dx$  for each particle type for a bin with residual range  $6(\pm 1)$  cm (right). The small difference between muon and pion PID is illustrated.

### 2.3.5 Reconstruction effects

Reconstruction algorithms use all three wire planes and the drift time for 3D track and event reconstruction. The quality of reconstruction is affected by two main factors that can be quantified with test beam data:

- The complexity of the event topology, which includes the number of objects overlapping in 2D projections and the number of possible object associations between 2D projections. The topology complexity depends on the energy of the incident particle. Hadronic showers collected with the test beam can provide data sample to assess the reconstruction algorithm performance and test its dependence on the incident particle energy.
- Orientation of the reconstructed object w.r.t. the readout wires and electron drift direction:
  - Tracks and cascades in the plane parallel or almost parallel to the wire planes have nearly identical hit drift time. These drift times are required for the 3D

reconstruction. Under real detector conditions reconstruction algorithms can show varying performance for this class of objects, especially in the presence of noise affecting hit time reconstruction.

- A 2D projection of objects aligned with the wires of one of the planes is strongly shortened, which limits the amount of information available to the reconstruction algorithm; the two other wire planes can be used for spatial reconstruction. However, the validation of the correctness of reconstruction, calculated from the 3D object projected to the third plane, is less efficient. The most important aspect of this issue is the use of all planes for the charge measurement. If the reconstructed object is aligned with collection wires then the calorimetric measurement has to be carried out with the signal from the induction planes. The additional shielding wire plane in the DUNE design will improve the quality of the bipolar induction plane signals. The test beam data will help with the calibration of these signals.
- Objects aligned with the drift field are projected onto a low number of wires and have a large span of drift time. The wire signals in these cases are significantly different than those from tracks at higher angles with respect to the drift field, and therefore require a dedicated signal processing algorithm to do hit reconstruction. Corrections for angular dependence of recombination will also need to be included in the calorimetric reconstruction and calibrated with real data.

Any reconstruction algorithm will depend on the particular choices in the TPC design. Therefore bench-marking our reconstruction algorithms with a prototype of the final design will be invaluable to understand the performance of reconstruction.

### 2.3.6 $e/\gamma$ separation

The search for a CP violation phase using  $\nu_e$  appearance in a  $\nu_\mu$  beam requires good electron/photon separation. Backgrounds originating from photons produced primarily from final state  $\pi^0$ 's must be identified and removed from the signal electron sample.

High energy photons can undergo two processes: pair production and Compton scattering. The dominant process for photons with energies of several hundred MeV or more is  $e^+ e^-$  pair production.  $e/\gamma$  discrimination for this process can be achieved using the beginning of the electromagnetic shower, where a single MIP is characteristic of electron energy deposition while two MIPs is consistent with a photon hypothesis. In the case where the photon Compton scatters, the two particles cannot easily be distinguished from the energy deposition pattern.

Electron-photon separation has been studied in LAr TPCs (ICARUS [23] and ArgoNeuT [24]). Fig. 8 shows estimated photon background rejection versus electron identification efficiency using simulated isotropic electron and photon event samples with the APA geometry configuration [1]. The results are found to be mildly dependent on incoming particle energy in the range of interest. Our studies indicate that rejection and efficiency depend on particular features of the geometry including wire pitch and plane orientation which affect the reconstruction. For example, a preliminary comparison of signal efficiencies for a simulated DUNE APA configuration with the ICARUS

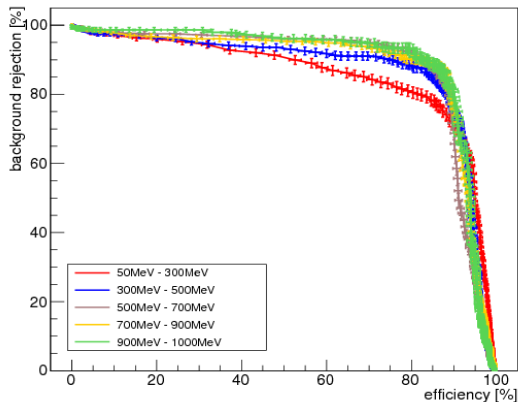


Figure 8: Photon background rejection versus electron identification efficiency for various energies, calculated for and normalized to samples which pass the reconstruction. The simulation was performed in APA design configuration (4.67 mm wire pitch, induction wires at  $\pm 35.7^\circ$  w.r.t. collection wires).

T600 geometry and averaged over the energy range 0.2-1.0 GeV shows a 10% higher efficiency for the 3 mm wire spacing used in ICARUS. The study does not yet include electron diffusion. Pure samples of electrons and photons in the sub-GeV energy range will be needed to tune the separation algorithms and to measure detector-dependent electron-photon separation efficiency and purity.

## 2.4 Other measurements

The DUNE experiment will be capable of addressing other physics beyond the long-baseline neutrino measurements with the unique massive underground LAr TPC. Event samples discussed here include those that support this rich array of additional physics goals.

### 2.4.1 Supernova and Michel electrons

Neutrinos produced in supernova burst (SNB) explosions are calculated to be in the few-to-30-MeV range. The DUNE Far Detector is expected to have unique sensitivity to the  $\nu_e$ 's from a SNB in our galaxy. The test beam cannot offer a sample of such low energy electrons, but Michel electrons produced by decaying stopped muons are ideal to calibrate electron response in the appropriate 10-50 MeV energy range. The requested sample of low energy muons will supply the 1400 Michel electrons required for a 1% calibration of electrons in this energy range. This sample can be compared to a similar Michel electron sample stemming from stopping cosmic muons.

### 2.4.2 Charge sign determination

It is not possible to determine the charge of the particle on an event by event basis with non-magnetized LAr TPC detectors. A statistical separation will be studied which will make use of differences in muon versus anti-muon capture cross sections and lifetime.

For the  $\mu^-$  we expect about 99.9% to be captured on argon whereas essentially all  $\mu^+$  decay [25]. Charge-sign tagged  $\nu_\mu$  samples may be useful to constrain exotic possibilities such as non-standard neutrino interactions which predict differences in the particle and anti-particle survival probabilities.

### 2.4.3 Proton decay sensitivity and background samples

The DUNE experiment in the deep underground location will seek to detect several modes of proton decay. In particular, a first ever LAr detector of this scale underground will primarily improve sensitivity to proton decays with final state kaons such as  $p \rightarrow K^+\bar{\nu}$ . Sensitivity to this process is studied in [26].  $K^+$  detection efficiency is estimated to be >97% in the appropriate momentum range (500-800 MeV/c). The kaon samples requested in Table 1 are needed to directly measure  $K^+$  PID and detection efficiency.

Obtaining low energy kaons will likely be difficult in this beamline. A sample of 13k beam kaons with 1 GeV/c momentum are requested to provide 2k stopping  $K^+$  track samples for PID studies. (Only 15% of  $K^+$  stop at 1 GeV/c.)

A sizable sample of protons ( $\sim 10^6$ ) are requested to study the possible background contributions to  $p \rightarrow K^+\bar{\nu}$ . This sample of protons are needed to quantify the possibility that an interacting proton is misidentified as stopping kaon. A proton interaction which produces neutrals and one charged pion (which is misidentified or subsequently decays to  $\mu$ ) can fake the final state kaon signal.

### 2.4.4 Anti-proton annihilation

A sample of anti-protons would be useful to calibrate the  $p\bar{p}$  annihilation process. This would provide input to exotic an baryon number violating process in which oscillation between neutron and anti-neutron occurs and results in a subsequent  $n\bar{n}$  annihilation. The modeling of  $p - \bar{p}$  annihilation could be studied and tuned on a low-energy  $\bar{p}$  beam sample and used to constrain the related modes expected for  $n\bar{n}$  annihilation. These events would be tagged in the mixed-mode beam. Events in the sub-GeV range would be the most useful for this purpose.

## 3 Single-Phase LAr Detector

### 3.1 DUNE detector plans

The far detector for the DUNE collaboration will be a series of four liquid argon TPCs, each in a cryostat that holds a fiducial/active/total LAr mass of 10.0/13.3/17.1 kt. The TPCs will be instrumented with a photon detection system. It is planned that the first 10 kt detector will be ready for installation in the 2022 timeframe. The design for the first 10 kt detector is a submerged wire plane-based TPC with electronic readout also in the liquid argon. Designs of this style are referred to as single-phase detectors as the charge generation, drift, and detection all occurs in the liquid argon phase. This style TPC features no charge amplification before collection, thereby making a very precise charge measurement possible.

To achieve DUNE’s goals, a detector is needed that is much larger than ICARUS, the largest LAr TPC detector built to date. The former LBNE developed a scalable far detector design shown in Fig. 9 that would scale-up LAr TPC technology by roughly a factor of 40 compared to the ICARUS T600 detector. To achieve this scale-up, a number of novel design elements need to be employed. A membrane cryostat typical for the liquefied natural gas industry will be used instead of a conventional evacuated cryostat. The wire planes or APAs will be factory-built as planar modules that are then installed into the cryostat. The modular nature of the APAs allow the size of the detector to be scaled up to at least 40 kt fiducial mass. Both the analog and digital electronics will be mounted on the wire planes inside the cryostat in order to reduce the electronic noise, to avoid transporting analog signals large distances, and to reduce the number of cables that penetrate the cryostat.

The scintillation photon detectors will employ light collection paddles to reduce the required photo-cathode area and thereby cost. Designs being considered are also more compact than the photomultiplier tubes solution used elsewhere.

Many of the aspects of the design are being tested in a small scale prototype at Fermilab but given the very large scale of the detector elements a full-scale test is critical. Since the recent formation of the new DUNE collaboration a combined detector design team is emerging. Ideas from this new collaboration have the potential to modify the detector design for the additional three far detector modules which are foreseen for DUNE. The detector design described here is the LBNE detector design chosen by the DUNE collaboration as the reference design for the first 10 kt detector module and also adopted as the basis for the DUNE-PT.

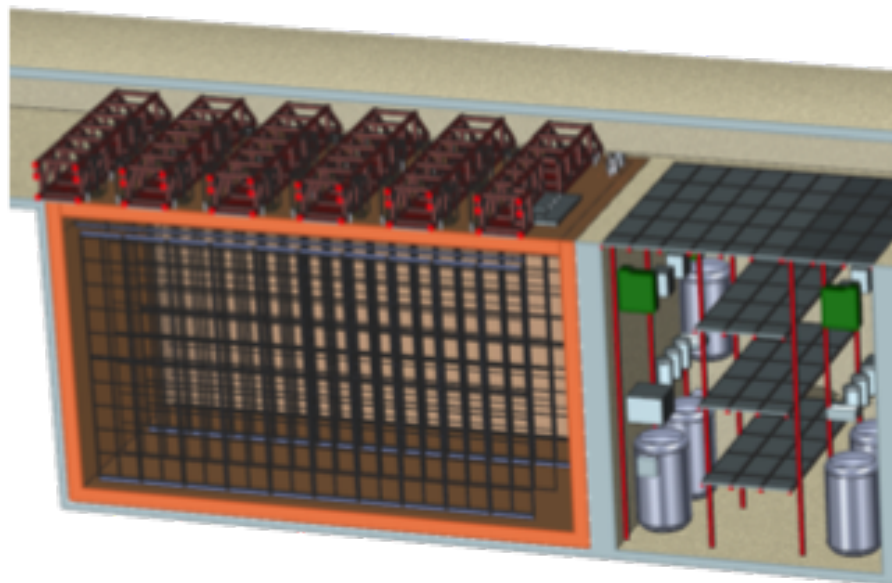


Figure 9: 3D model of the design for the first DUNE single-phase detector. Shown is a 5 kt fiducial volume detector which would need to be lengthened for the 10 kt design. The present DUNE plan calls for the construction of four 10 kt detectors.

The engineering goals of the single-phase APA/CPA detector test can be broken into five broad categories:

1. TPC performance, mechanical and electrical verification,
2. photon detection light yield verification,
3. calibration strategy verification,
4. argon contamination mitigation verification,
5. production and installation procedure verification

The goals related to mechanical testing are to test the integrity of the detector. In the current design, each APA measures 2.3 m by 6.0 m and includes 2560 wires and associated readout channels. Given the complexity of these assemblies, a test where the detector can be cooled down and tested under operating conditions is highly advisable prior to mass production. The mechanical support of the APAs can be tested to verify that the mechanical design is reliable and will accommodate any necessary motion between the large wire planes. The impact of vibration isolation between the cryostat roof and the detector can also be tested. Finally, an improvement over existing cryostat designs is the possibility to move the pumps external to the main cryostat. This will reduce any mechanical coupling to the detector and also greatly improve both reliability and ease of repair.

The electrical testing goals are to insure that the high voltage design is robust and that the required low electronic noise level can be achieved. As the detector scale increases so does the capacitance and the stored energy in the device. The design of the field cage and high voltage cathode planes needs to be such that HV discharge is unlikely and that if the event occurs no damage to the detector or cryostat results. The grounding and shielding of large detectors is also critical for low noise operation. By testing the full scale elements one insures that the grounding plan is fully developed and effective. Large scale tests of the resulting design will verify the electrical model of the detector.

Research at Fermilab utilizing the Materials Test Stand [27] has shown that electronegative contamination to the ultra-pure argon from all materials tested is negligible if the material is immersed in the liquid argon. This implies that the dominant source of contamination originates from the gas ullage region and the room temperature connections to the detector. Careful design of the ullage region to insure that all surfaces and feedthroughs are cold is expected to greatly reduce the sources of contamination over what exists in present detectors.

## 3.2 DUNE-PT

This section presents the design details of a single-phase prototype detector based on the design by the former LBNE collaboration [28]. The DUNE detector design is modular and the DUNE-PT will be constructed from modular components of exactly the same design.

The TPC consists of alternating anode plane assemblies (APAs) and cathode plane assemblies (CPAs), with field-cage panels enclosing the four open sides between the anode and cathode planes. Fig. 10 shows a sectioned view for the planned TPC by itself and inside the cryostat at CERN. A 500 V/cm uniform electric field is created in

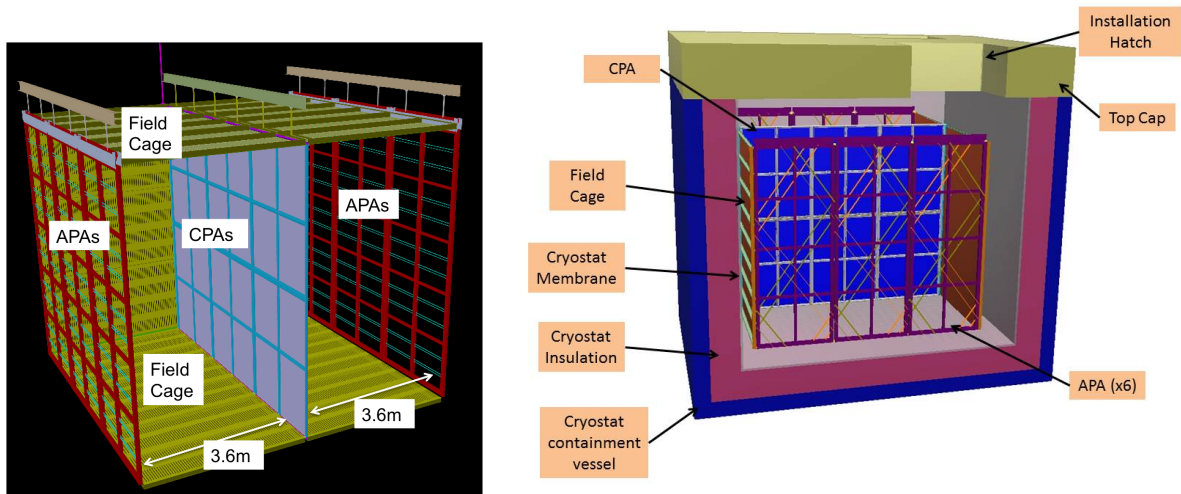


Figure 10: 3D model of the CERN single-phase detector TPC (left) and inserted in the cryostat (right).

the volume between the anode and cathode planes. A charged particle traversing this volume leaves a trail of ionization. The electrons drift toward the anode plane, which is constructed from multiple layers of sense wires, inducing electric current signals in the front-end electronic circuits connected to the wires.

The TPC will be assembled from elements that are of the same size and materials as those planned for the first DUNE far detector module.

The overall size of the TPC has been determined based on the desired particle containment in order to address the required physics measurements (see Section 2). The TPC will have an active volume that is 3 APAs long and consists of two drift volumes with a drift length of 3.6 m each (see Fig. 10). The APAs have an active (total) area measuring 2.29 m (2.32 m) wide and 5.9 m (6.2 m) high. The combination of the three APAs determines the overall TPC length to be 7.0 m. There will be a CPA in the center between the two rows of APAs. The overall width of the TPC will be determined by the 7.4 m combination of the drift distances and the total thicknesses of the two APA planes and the CPAs. The overall height of the TPC is determined by the height of the APA which is 6.2 m. The TPC dimensions are summarized in Table 2. The minimum internal size of the cryostat is also indicated in Table 2 and was determined by adding the necessary mechanical and electrical clearances to the computed size of the TPC.

Component	dimensions [m]
APA (active)	2.29( <i>wide</i> ) $\times$ 5.9( <i>high</i> )
APA (external)	2.32( <i>wide</i> ) $\times$ 6.2( <i>high</i> )
TPC (active)	7.0( <i>long</i> ) $\times$ 7.2( <i>wide</i> ) $\times$ 5.9( <i>high</i> )
TPC (external)	7.3( <i>long</i> ) $\times$ 7.4( <i>wide</i> ) $\times$ 6.2( <i>high</i> )
cryostat (internal)	8.9( <i>long</i> ) $\times$ 7.8( <i>wide</i> ) $\times$ 8.1( <i>high</i> )

Table 2: Dimensions of DUNE-PT.

Along with the APAs and CPAs, the TPC will include a field cage that surrounds

the entire assembly to ensure a uniform drift field in the TPC’s active volume. -

All of this will be supported by rows of I-beams supported from a mechanical structure above the cryostat. The hangers for these I-beams will pass through the insulated top cap. There will be a series of feedthrough flanges in the top cap of the cryostat to bring in and take out services for the TPC. One HV feed-through is foreseen for the CPA row and one signal feed-through for each of the APAs.

The design also foresees the option to have the two APA rows mounted at 2.5 m from the central CPA each. A reduced drift distance between the APA and CPA represents a deviation from the DUNE far detector design but is potentially very useful in order to lessen the impact of space charge effects. Due to the operation of DUNE-PT on the surface, space charge effects (discussed in Section 5) are expected to be larger than for underground operation at SURF. We foresee to calibrate out any space charge effects for a 3.6 m drift distance using laser beam calibration and cosmics. At the same time we maintain the possibility for a second test with reduced drift length if the uncertainties associated with our calibration limit the precision of measurements. The cryostat would have to be emptied and the planes shifted to the 2.5 m drift distance.

### 3.2.1 Anode plane assemblies (APAs)

Each APA (Fig. 11) is instrumented with 3 layers of signal wires, one collection plane with vertical wires and two induction planes with wires at  $\pm 35.7^\circ$  to the vertical. An additional outer grid plane helps maintain the field. The overall dimensions of the active area are 2.3 m wide and 5.9 m long. The dimension of the wire planes were selected to fit down the Ross shaft at SURF, the future location of the DUNE far detector, be compatible with a standard HiCube transport container, and allow construction from readily available materials. The wire angle was selected so that a given angled induction wire will not overlay any longitudinal collection wire more than once in order to reduce ambiguities caused by the wrapped wire construction. Partial wire layers are shown in Figure 11 at the bottom. With a wire pitches of 4.67 mm (diagonal layers) and 4.79 mm (straight layers), the total number of readout channels in an APA is 2560. The grid layer is not depicted in Fig. 11 for clarity. The underlying structure of each APA is a framework of rectangular, stainless steel tubing. The side and bottom edges of the frame are lined with multiple layers of fiberglass circuit boards, notched along the edges to support and locate the wires that cross the APA face. A set of FR4 combs are glued to the APA frame to capture the wires at regular intervals. The front-end electronics boards are mounted at the top end of the frame and protected by a metal enclosure.

The distance between wire planes is 4.8 mm (3/16 in) matching the standard printed circuit board thickness, and are designed to maintain optimal signal formation. The four wire planes will be electrically biased so that electrons from ionizing-particle tracks completely drift past the first three planes and are collected by the fourth plane. Calculations show that the minimum bias voltages needed to achieve this goal are  $V_G = -665$  V,  $V_U = -370$  V,  $V_V = 0$  V and  $V_X = 820$  V respectively (where G, U, V, and X are the wire-layer labels from outside in, towards the frame). It is convenient to set one of the wire planes to ground so that the wires can be DC coupled to the front-end readout electronics. In this instance, the V wire plane is set to ground potential to reduce the maximum bias voltages on the other wire planes, and enable the use of lower voltage

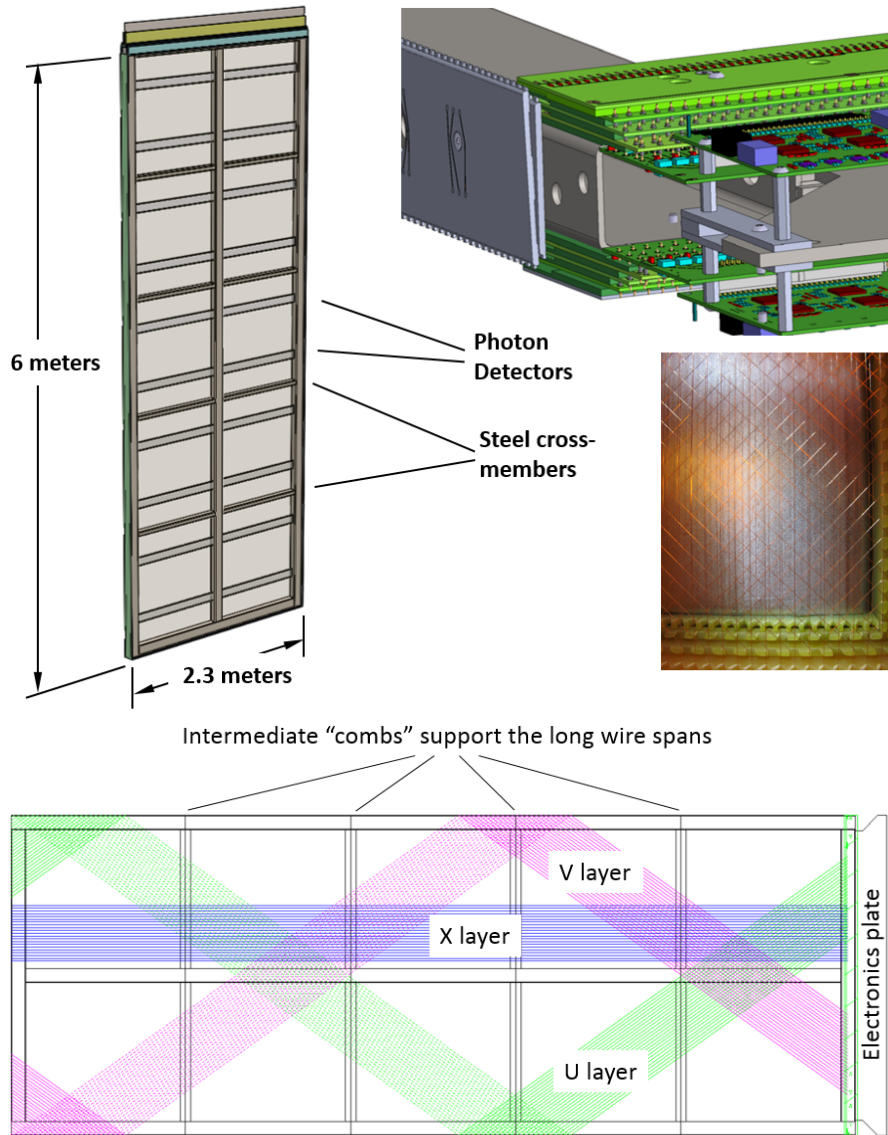


Figure 11: Clockwise from left: A full size APA, an APA corner showing the electronics boards, an APA lower corner photo showing wires and edge boards, and a figure showing the wire orientations and the placement of wire aligning combs.

rated AC coupling capacitors. A grounded mesh plane, located 4.8 mm behind the collection (X) plane, prevents the electric field around this set of wires from being distorted by the metal frame structure and the wires on the opposite side of the frame. It also shields the sensing wires from potential EM interferences from the photon detectors (Fig. 12) mounted within the frame. The mesh should have a wire pitch less than 2 mm to ensure a uniform electric field while maintaining good optical transparency.

### 3.2.2 CPA and field cage

Each cathode plane (Fig. 13) is constructed from 6 identical CPA (cathode plane assembly) modules and two sets of end pieces. Each CPA is about half the size of an APA

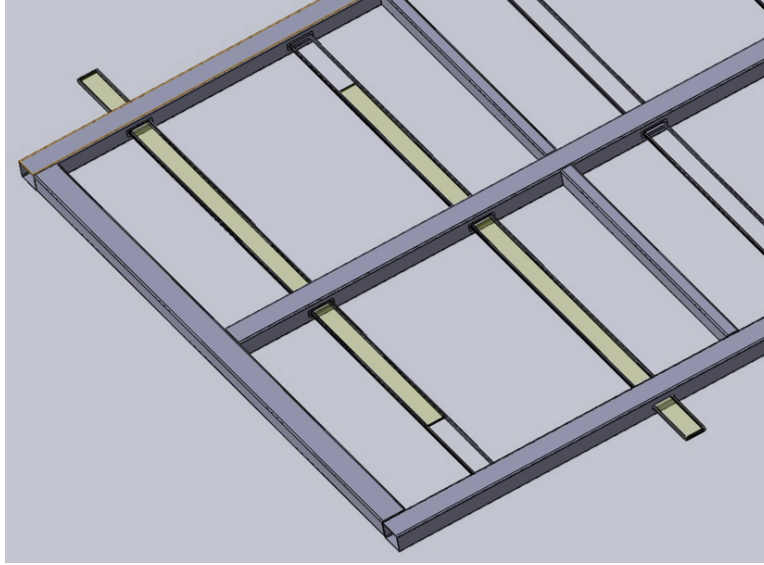


Figure 12: Photon detectors are mounted within the frame, between the wires on the two sets of four wire layers. The APA is built so that the photon detectors can be installed through slots in the side of the APA after the APA wires are installed. The wires that would cross these slots are routed around using copper traces on the edge boards.

(2.3m  $\times$  3.1m) for ease of assembly and transport. The CPA is made of a stainless-steel framework, with 4 pieces of thin FR4 sheets mounted in the openings. A receptacle for the HV feedthrough is attached to the upper corner of a cathode plane toward the roof entrance side to mate with the HV feedthrough in the cryostat ceiling.

The FR4 sheets on the CPAs are treated with layers of high resistive coating on both sides. The resistivity of the coating will be chosen such that the surface potential does not deviate significantly with the ionization current from the cosmic rays, and forms a relatively long time constant to dissipate the stored energy on each sheet in case of a high voltage discharge. This long RC time constant will also reduce the peak current injected into the front-end electronics in a HV discharge.

The high flux of cosmic rays combined with very low drift velocity of positive ions in the liquid argon will result in non-negligible space charge distortions in the TPC [29]. In addition, the positive ions could build up further if the ion motion is slowed or stalled by counter flow in the LAr. Preliminary Computational Fluid Dynamics (CFD) analysis [30] have shown that solid cathodes in the cryostat result in LAr flow pattern that neither causes excess positive ion buildup, nor degrades the LAr purity.

To achieve a 500 V/cm drift field over a 3.6 m distance, the bias voltage on the cathode plane must reach  $-180$  kV. One high voltage power supply (150 – 200 kV) and one HV feedthrough will be needed for the cathode plane. The HV feedthroughs are based on the ICARUS design [6], but are modified to further improve the stability at higher voltages.

The field cages are constructed using copper-clad FR4 sheets reinforced with fiber glass I-beams to form panels of 3.6 m  $\times$  2.3 m in size for the top and bottom modules, and 3.6 m  $\times$  2 m modules for the sides. Parallel copper strips are etched or machined on the FR4 sheets. Strips are biased at appropriate voltages through a resistive divider

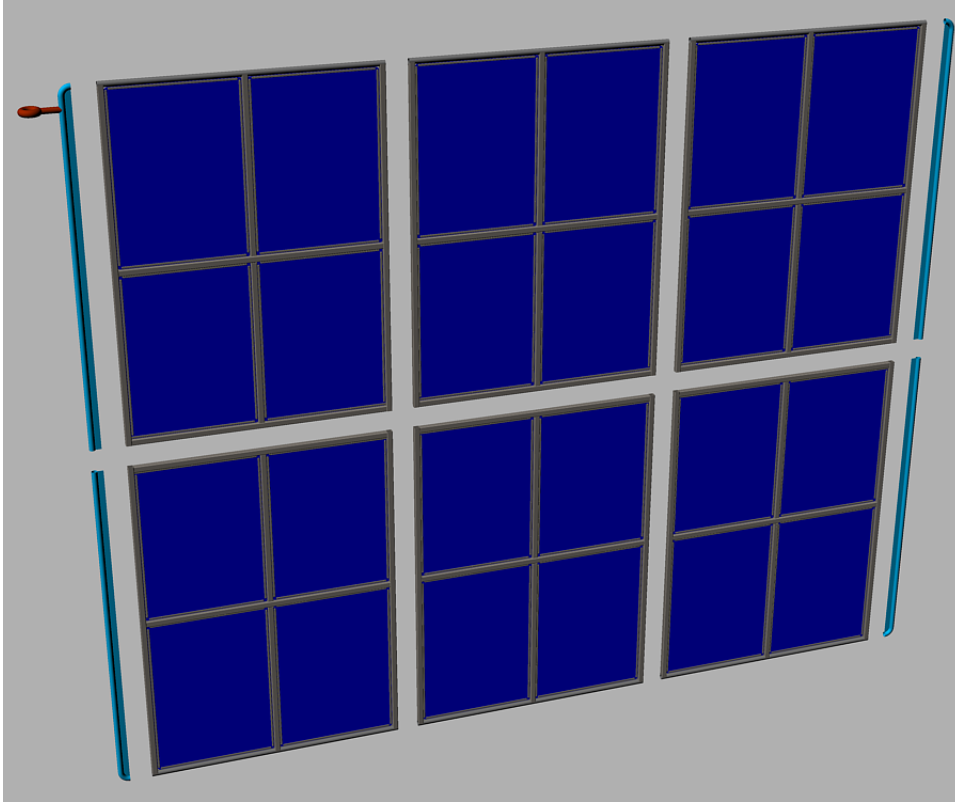


Figure 13: Exploded view of a cathode plane constructed from 6 CPA modules and 4 end pieces. The facing material on the CPA is highly resistive to minimize the peak energy transfer in case of a HV breakdown.

network. These strips will create a linear electric-potential gradient in the LAr, ensuring a uniform drift field in the TPC’s active volume.

The left of Fig. 14 shows a section of the field cage in the 35 t TPC as it was being assembled. The 35 t TPC test results will inform us whether we should improve upon the current design, or consider alternate designs.

In the event of HV discharge on the cathode or the field cage, the voltage differential between neighboring field cage strips near the discharge electrode will be very high for a brief moment. This over voltage condition could cause damage to the field cage electrode and the resistors installed between strips. To minimize such risk, varistors or Gas Discharge Tubes (GDT) will be installed between the field cage strips in parallel with the resistors to prevent excess voltage transient between the electrodes.

In order to test the installation concept of the far detector, the top and bottom field cage modules will be attached to the mating CPA through hinges. This combined assembly will be installed into the cryostat and the field cage module opens to connect the CPA and the APA both mechanically and electrically.

### 3.2.3 Photon detection system

The photon detection system (PDS) of the DUNE far detector will utilize liquid argon scintillation light. The system will be used to trigger on non-beam events and to deter-



Figure 14: A section of the field cage in the 35 t TPC.

mine the prompt event time for both non-beam and beam events. Timing information will be useful in determining the  $t_0$  of cosmic rays, including those which overlap with beam events and events from radiological decays. This timing information allows proper spatial event reconstruction, including the reconstruction and rejection of background events.

While the TPC will have spatial resolution that is far superior to a photon detection system, it offers no intrinsic precise determination of the event time. However, the photon detection system can determine the start of an event occurring in the TPC volume (or entering the volume) to about 6 ns. For beam-triggered events the performance of the photon detection timing information can be crosschecked and evaluated during the detector beam test. In addition to providing trigger functionality, the PDS may be able to improve the event energy reconstruction by providing drift length dependent corrections to energy loss of the drifting electrons. In the absence of an external electric field, a charged particle passing through liquid argon will produce about 44,000 photons ( $\lambda = 128$  nm) per MeV of deposited energy. At higher electric drift fields the number of photons will be smaller due to reduced recombination, but at 500 V/cm the yield is about 20,000 photons per MeV. Roughly one-third of the photons are prompt, 2-6 ns, and two-thirds are generated with a long time constant of 1.1-1.6  $\mu$ s. LAr is highly transparent to the 128 nm VUV photons with a Rayleigh scattering length and absorption length of  $55 \pm 5$  cm [33] and  $>200$  cm [34] respectively. Nitrogen contamination of the liquid argon can reduce the attenuation length. The relatively large light yield makes the scintillation process an excellent candidate for triggering and determination of  $t_0$  for non-beam related events. Detection of the scintillation light may also be helpful in background rejection and possibly provide improvements for energy reconstruction.

Several prototypes of photon detection systems for single phase liquid argon detectors have been developed by the former LBNE photon detector group over the past few years. There are currently four prototypes under consideration for use in the first module of the DUNE far detector, a baseline design along with three alternate designs. A decision on the design to be deployed in the CERN test will be made in late 2015. DUNE-PT provides the first full scale test of the photon detectors which will be fully integrated into a full scale APA.

The present reference design for the photon detection system is based on acrylic bars that are 200 cm long and 7.6 cm wide, which are coated with a layer of tetraphenyl-

butadiene (TPB). The wavelength shifter converts incoming VUV (128 nm) scintillation photons to longer wavelength photons which are characterized by an emission spectrum with a peak wavelength of 430 nm. About 50% of the converted photons will be emitted into the bar. A fraction of the wavelength-shifted optical photons are internally reflected to the bar's end where they are detected by SiPMs whose QE curve is well matched to the 430 nm wavelength-shifted photons. All PD prototypes are currently using SensL MicroFC-6K-35-SMT 6 mm  $\times$  6 mm devices [35].

A full 6 m long APA will be divided into 5 bays with 2 PD modules (paddles) instrumenting each bay. The paddles will be inserted into the frames after the TPC wires have been strung allowing final assembly at the CERN test location. Two alternative designs are also under consideration.

One alternate design attempts to increase the geometrical acceptance of the photon detectors by using large acrylic TPB coated plates with imbedded WLS fibers for readout. In this design the number of required SiPMs and readout channels per detector area would be significantly reduced. This will keep the overall cost for the photon detection system at or below the present design while increasing the geometrical acceptance. The prototype consists of a TPB-coated acrylic panel embedded with a S-shaped wavelength shifting (WLS) fiber. The fiber is read out by two SiPMs, coupled to either end of the fiber, and serves to transport the light over long distances with minimal attenuation. The double-ended fiber readout has the added benefit to provide some position dependence to the light generation along the panel by comparing relative signal sizes and arrival times in the two SiPMs.

The third design under consideration was motivated by increasing the attenuation length of the PD paddles and allowing collection of 400 nm photons coming from anywhere in the active volume of the TPC. The fiber-bundle design is based on a thin TPB coated acrylic radiator located in front of a close packed array of WLS fibers. This concept is designed so that roughly half of the photons converted in the radiator are incident on the bundle of fibers, the wavelength shifting fibers are Y11 UV/blue with a 4% capture probability. The fibers are then read out using SiPMs at one end. The Y11 Kuraray fibers have mean absorption and emission wavelengths of about 440 nm and 480 nm respectively. The attenuation length of the Y11 fibers is given to be greater than 3.5 m at the mean emission wavelength, which will allow production of full-scale (2 m length) photon detector paddles.

The PD system tested at the CERN neutrino platform will be based on technology selected later in 2015. The technology selection process will be based on a series of tests planned for 6 months utilizing large research cryostats at Fermilab and Colorado State University. The primary metric used for comparison between the three technologies will be photon yield per unit cost. In addition to this metric, PD threshold and reliability will also serve as inputs to the final decision. A technical panel will be assembled to make an unbiased decision.

### 3.2.4 TPC and PDS readout

A single APA has 2560 sense wires that need to be readout. In order to minimize the capacitance, the preamplifier noise, and the number of penetrations through the cryostat, the Front-End (FE) electronics boards of the **TPC electronics** digitize the signals and

are mounted in the cryostat. They are located on one end of the wire frame just outside of the active TPC volume. A single APA is readout by 20 sets of FE readout boards with each FE reading in 128 wire channel inputs (40 U-view + 40 V-view + 48 X-view) and each FE transmitting 4 outputs through the cryostat to back-end electronics.

The present design has a maximum wire length of 7.3 m (induction planes) with a corresponding capacitance of 164 pF and an expected intrinsic noise of 400 electrons. The preamplifiers include shaping circuits, and are implemented in 16 channel FE ASICs, which couple directly to 16 channel, 12 bit ADC ASICs operating at 2 MS/s, which include a 1:8 multiplexing stage. The ADCs are read out by a commercial FPGA, which provides an additional factor of 4 in multiplexing. This level of multiplexing is low enough for transmitting the entire raw data stream, while also being high enough that the number of signal lines is actually smaller than the number of the various power and control lines, and therefore easily manageable by a small number of feedthroughs. Neither zero suppression nor data compression is implemented at the level of the cold readout electronics. Not only does this greatly simplify the cold electronics design, but it also automatically satisfies the requirement that the system be capable of such raw readout. The FPGAs transmit the data via high-speed (1 Gbps) serial links to the DAQ system. For the final detector it is expected that a dedicated digital control and data transmission ASIC (COLDATA) will be developed which replaces the commercial FPGA. While the COLDATA is well under way, it is not expected to be available in time for the CERN test, which will instead make use of the proven FPGA technology. While serious doubts regarding the longevity of commercially-available FPGAs at LAr temperatures strongly argues against their use in the Far Detector, where reliability over 15-20 years is required, this is not a concern for the CERN test, where the proven FPGA lifetime of at least a year is adequate.

The front end electronics is organized as a stack of three boards comprising the FE Mother Board assembly (FEMB), which mounts directly on the APA. First is the Analog Mother Board, on which are mounted the FE and ADC ASICs. Second and third are the FPGA and SERDES Mezzanine Boards, themselves mounted on the Analog Mother Board. Each FEMB has eight sets of FE and ADC ASICs and instruments 128 wires. A Faraday cage (FC) covers the end of the APAs to shield the electronics from ambient noise. The FC also serves to prevent any Ar gas-bubbles from LAr boiled by the electronics' heat from entering the active TPC volume. Figure 15 shows a schematic of the cold electronics.

Besides the high-speed signal cable, which is a twin-axial cable bundle manufactured by GORE, there are cable bundles for low-voltage power, wire-bias voltages, and various slow controls and monitoring. The cable bundles will be connected through a feedthrough on the roof of the cryostat.

The primary interface between the TPC front-end electronics (FE) and the DAQ sub-system consists of an ATCA-based system of RCEs (Reconfigurable Cluster Elements). The RCE system receives the serialized raw data from the FE, performs zero-suppression on it, and packetizes and transmits the resulting sparsified data to a back-end data farm for event building and further processing. Additionally, the RCE system transmits timing and control signals to the FE as well as forwarding configuration data to them at start-up.

The RCE system consists of the following components: a commercial ATCA shelf

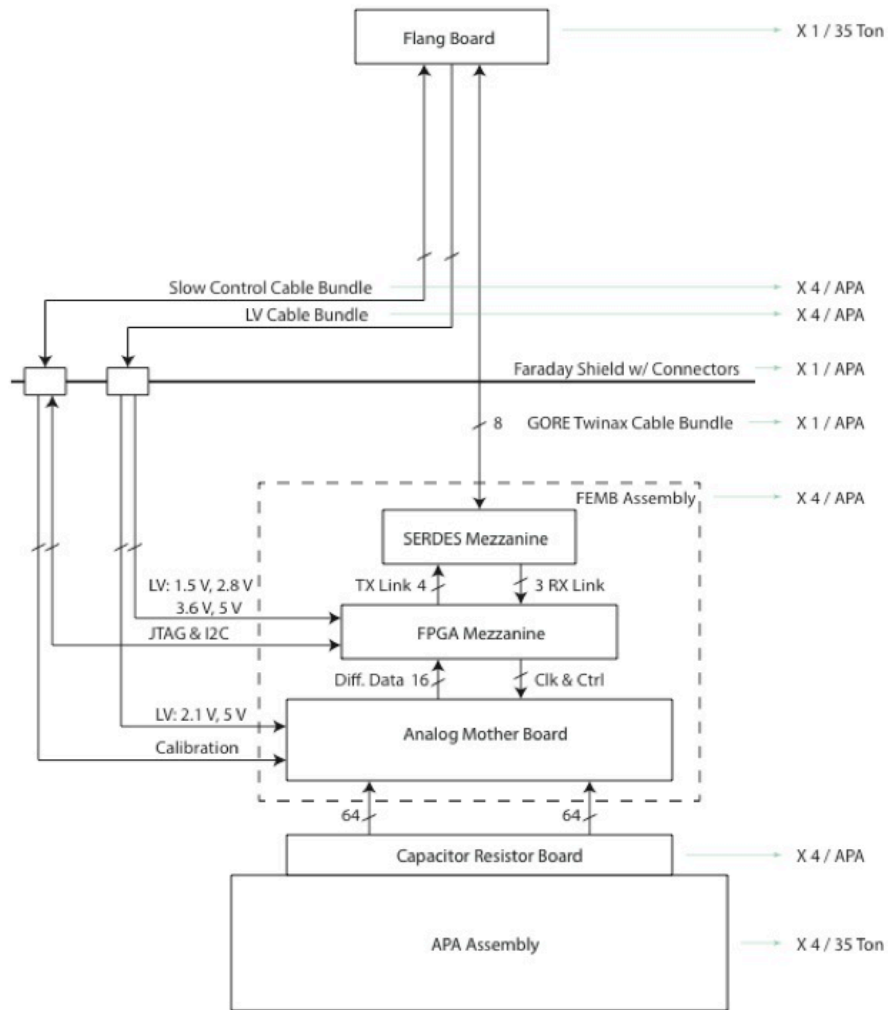


Figure 15: Layout of the TPC cold front end (FE) electronics..

(2-, 6-, or 14-slot), a Cluster-On-Board (COB) which is the "front board" in ATCA terms, and a Rear-Transition-Module (RTM) which is the "rear board". A schematic of the system is shown in Fig. 16. The COB is a custom board, developed by SLAC, which holds the processing power of the system. The COB (see Fig. 16) consists of 5 bays for holding daughter boards, an onboard 10-GbE switch, and both 10- and 1-Gb ethernet connections for communications with the back-end system. Four of the daughter-board bays are for Data Processing Modules (DPM), each of which can hold up to two RCEs. The RCE is the core processing unit of the system; it is made up of a modern SoC (currently, the Xilinx Zynq-7045) with multiple high-speed I/O ports (up to 10-Gbps each) and external DRAM and flash memory controllers. The other bay on the COB contains the Data Transmission Module (DTM) which is responsible for distributing timing and trigger information to and between the DPMs.

While the COB hardware is application agnostic, the RTM is application specific. The RTM provides the mechanical interface between the front-end (or, in our case, the flange electronics) and the back-end, as well as other external sources such as the timing

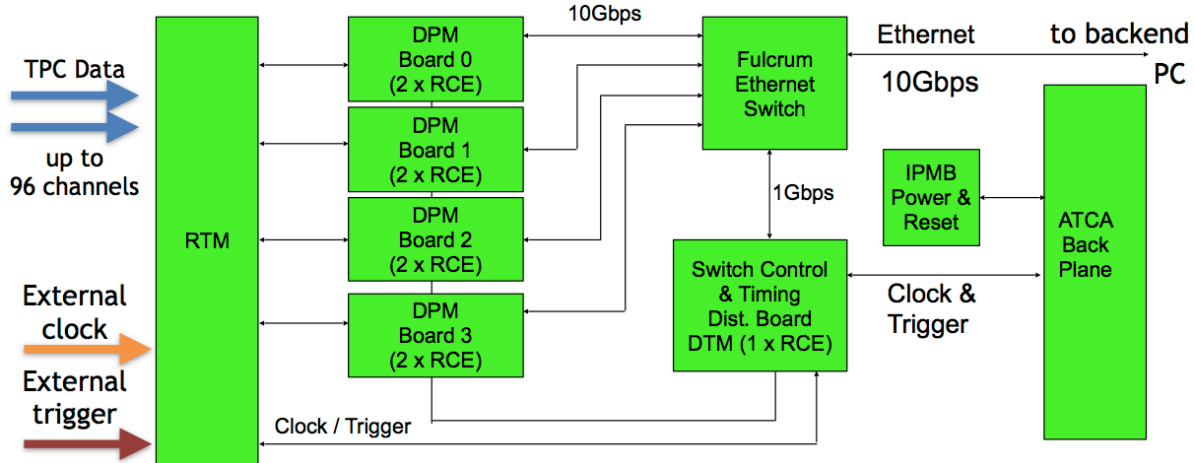


Figure 16: Top: Schematic for the TPC DAQ system. Bottom: The COB (left of the large connectors) and RTM (right).

or trigger systems. In this case we will use fiber optic connections between the flange and the TPC DAQ using 8 12-channel (full duplex) CXP connectors on the RTM.

With the assumption that each cold FE board multiplexes its 128 wire channels to 4 outputs at 1-Gbps each, the non-zero suppressed data for 1 APA can be fed into a single COB (containing 8 RCEs). Each RCE would receive data from 2 FE boards, perform zero-suppression, and send the result to the back-end.

The **PDS front-end electronics** resides outside of the cryostat in instrumentation racks. A custom module for receiving SiPM signals has been designed and built. The module also performs signal processing in the front-end as preprocessing for trigger and DAQ. The module is called the SiPM Signal Processor (SSP) and consists of 12 readout channels packaged in a self-contained 1U module. Each channel contains a fully-differential voltage amplifier and a 14-bit, 150-MSPS ADC that digitizes the waveforms received from the SiPMs. There is no shaping of the signal, since the SiPM response is slow enough relative to the speed of the digitization to obtain several digitized samples of the leading edge of the pulse for the determination of signal timing. Digitized data is processed by a Xilinx Artix-7 Field-Programmable Gate Array (FPGA). The use of the FPGA processing allows for a significant amount of customization of the SSP operation.

### 3.2.5 DAQ, Slow control and monitoring

The DAQ back-end software will merge data to form events from the TPC, photon detector and beam detector readouts using the artDAQ data acquisition toolkit using a farm of commercial computers connected with an Ethernet switch. ArtDAQ is in use on several experiments at Fermilab. We are using it on the 35 t prototype, so we will have considerable experience by the time of the CERN test.

The data collection for the CERN test will operate in a mode similar to that foreseen for the underground detectors. In order to collect data from non-beam interactions such as proton decay candidates or atmospheric neutrinos, data will be continuously read in to the artDAQ data receiver nodes and processed through the artDAQ system in quanta corresponding to time intervals fixed from the time of the beginning of the run. These are then transferred through the switch to a set of event building nodes which work in parallel, each node receiving all the data from all the detectors for the time intervals it is responsible for processing. There will be 32 parallel incoming data streams from the TPCs and 16 streams from the photon detectors. There will be an additional stream from the trigger board (similar to the board used by 35 t detector) which will receive input of the spill gate, warning of extraction, and pattern-unit bits from cosmic muon trigger counters and other beamline instrumentation which are described in Sections 5 and 6.2, respectively.

Synchronisation across all the input sources is essential in order that artDAQ can bring together the data from the input streams correctly for processing by the event building nodes. The data receiver nodes will provide overlap by repeating the data at the boundaries of the time intervals so that a particle whose data spans two time intervals can be collected. The time synchronization is provided to the RTM back-module on the LArTPC readout crates, to the SSP photon detector readout and to the trigger board from a GPS based time synchronization distribution system originally designed for the NOvA experiment. This system includes functionality to calibrate and correct for the cable delays, and to send synchronization control signals to the readout at predetermined times.

The event building nodes will select time regions of interest within the time intervals they are processing and form these into events to be written to disk. The algorithms to select the events may be as simple as looking for a trigger bit in the trigger board data stream, or may involve looking for self-triggered events in the LArTPC data. An aggregation task, which is part of artDAQ will handle the parallelized event building processes by merging the output events into a single stream and writing them to disk. To avoid oversized output data files, when a predetermined file size is reached, the aggregator will switch to writing to a new file.

Improved versions of the software systems which are being prototyped at the 35 t test will be available for the CERN test including (a) Run control which controls and monitors the DAQ processes and allows run starts and stops to be performed by the operator (b) online monitoring (c) slow control of voltages and temperatures being used by the electronics. The trigger board includes facilities for generating calibration pulses and for identifying the event times of the calibration events.

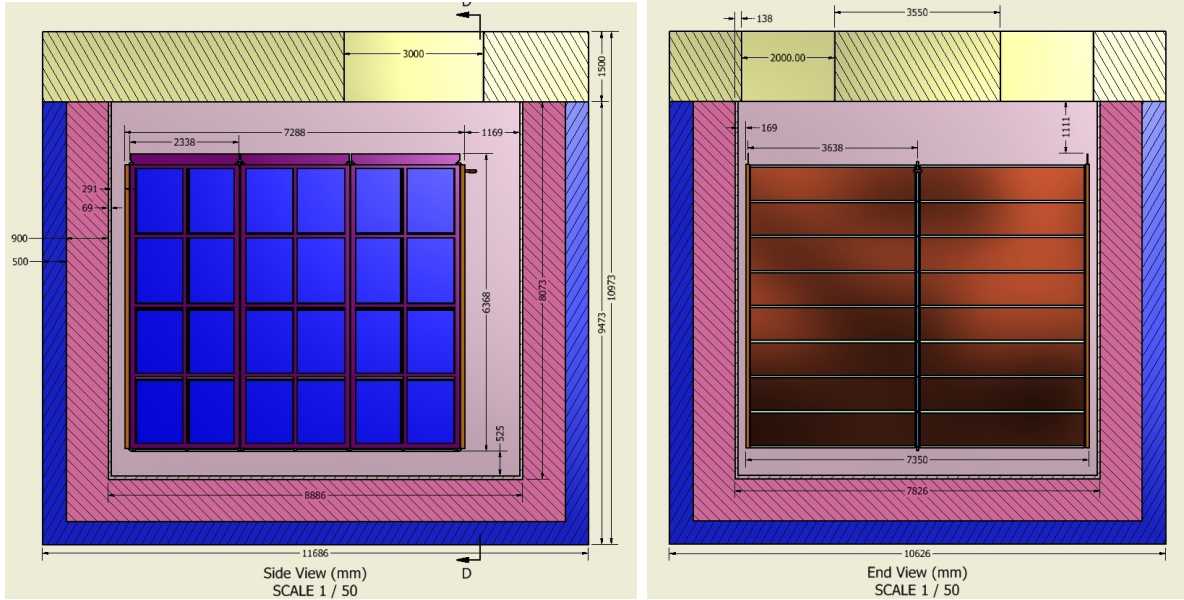


Figure 17: Side (left) and end (right) views of cryostat

## 4 Cryostat and Cryogenics System

### 4.1 Cryostat

DUNE-PT will use a membrane tank technology supported by an outer steel structure.

The minimum internal size of the cryostat is determined by the size of the TPC. At the bottom of the cryostat there needs to be a minimum of 0.36 m between the frame of the CPA and the closest point on the stainless steel membrane. This is to prevent high voltage discharge between the CPA and the electrically grounded membrane. It is foreseen that there would be some cryogenic piping and instrumentation under the TPC. There is a height allowance of 0.165 m for this. There will be access and egress space around the outside of the TPC and the membrane walls. On two sides, 0.15 m of space is reserved for this. The front will have 0.36 m and the back, where piping and instrumentation for the cryogenic system will be located, 1.20 m.

The support system for the TPC will be located outside the cryostat roof, with a bridge connected to the floor. The plan is to model the space similar to what is planned for the far site TPC. There will be 0.82 m of ullage space. In order to prevent high voltage discharge, the upper most part of the CPA needs to be submerged a minimum of 0.5 m below the liquid argon surface. The top of the TPC will be separated from the membrane by a minimum of 1.1 m.

Adding all of these to the size of the TPC yields the minimum inner dimensions of the cryostat. A minimally-sized cryostat would have inner dimensions of 8.9 m (length), 7.8 m (width) and 8.1 m (height). This assumes the TPC will be positioned inside the cryostat with the CPAs and end field cages parallel to the walls of the cryostat. Figure 10 shows a 3D view of the detector inside the cryostat and Figure 17 shows side and end views of the cryostat, respectively. The beam window design is still being worked on

and may lead to minor modifications if any of the current boundaries conditions listed above is violated.

The cryostat has an inner volume of 483 m<sup>3</sup> and can contain 673 t of LAr. The cryostat will use a steel outer supporting structure with a metal liner inside to isolate the insulation volume, similar to the one of the dual phase WA105 detector, the 1 × 1 × 3 m<sup>3</sup> prototype and to the Fermilab Short-Baseline Near Detector [36]. The support structure will rest on I-beams to allow for air circulation underneath in order to maintain the temperature within the allowable limits. The proposed design encompasses the following components:

- steel outer supporting structure,
- main body of the membrane cryostat (sides and floor),
- top cap of the membrane cryostat,
- beam windows.

A membrane cryostat design commonly used for liquefied natural gas (LNG) storage and transportation will be used. In this vessel a stainless steel membrane contains the liquid cryogen. The pressure loading of the liquid cryogen is transmitted through rigid foam insulation to the surrounding outer support structure, which provides external support. The membrane is corrugated to provide strain relief resulting from temperature related expansion and contraction. The vessel is completed with a top cap that uses the same technology.

Two membrane cryostat vendors are known: GTT (Gaztransport & Technigaz) from France and IHI (Ishikawajima-Harima Heavy Industries) from Japan. Each one is technically capable of delivering a membrane cryostat that meets the design requirements for this detector. To provide clarity, only one vendor is represented in this document, GTT; this is for informational purposes only. Figure 18 shows a 3D model of the GTT membrane and insulation design.

To minimize the contamination from warm surfaces, during operation the temperature of all surfaces in the ullage shall be lower than 100 K. It has been observed in the Materials Test Stand (MTS) and the Liquid Argon Purity Demonstrator (LAPD) at Fermilab that the outgassing is significantly reduced below 100 K [37]. A possible way to achieve this requirement is to spray a mist of clean liquid and gaseous argon to the metal surfaces in the ullage and keep them cold, similar to the strategy that was developed for the cool down of the 35 t prototype.

The top plate will contain two hatches for the installation of the TPCs; it will also contain a manhole to enter the tank after closing the hatches, and several penetrations for the cryogenic system and the detector.

The cryostat design for the CERN prototypes includes technical solutions that are of interest for the future needs of the DUNE program. For example the use of a cold ullage (<100 K) to lower the impurities in the gas region, and of a LAr pump outside the cryostat to minimize the effect of noise, vibration and microphonics to the TPC inside the liquid argon volume. The design parameters for the DUNE-PT cryostat can be found in the Appendix.

# GST<sup>®</sup> Containment System

## AS A PRIMARY BARRIER :

### a flexible (1.2mm) stainless steel membrane

The double network of corrugations absorbs the thermal contractions due to the very low temperature of the LNG.



## Insulating panel

The thickness of the panels can be adjusted to provide a large range of boil-off rates according to the operator's requirements (typically 0.05% per day).

## Plywood

## Reinforced polyurethane foam

## AS A SECONDARY BARRIER :

### a composite laminated material

This consists of a thin sheet of aluminium between two layers of glass cloth and resin. In the event of a failure of the primary membrane, it prevents the build-up of stress concentrations on concrete corner and ensures the liquid tightness of the concrete wall.

## Reinforced polyurethane foam

## Plywood

## Mastic

## Post-tensioned concrete covered by a moisture barrier

The outer concrete container provides the *structural resistance* to internal (LNG hydrostatic & dynamic pressure, and vapour gas pressure) and external (wind, snow, ice) loads. A moisture barrier, applied on its inner side, prevents moisture from entering the tank.

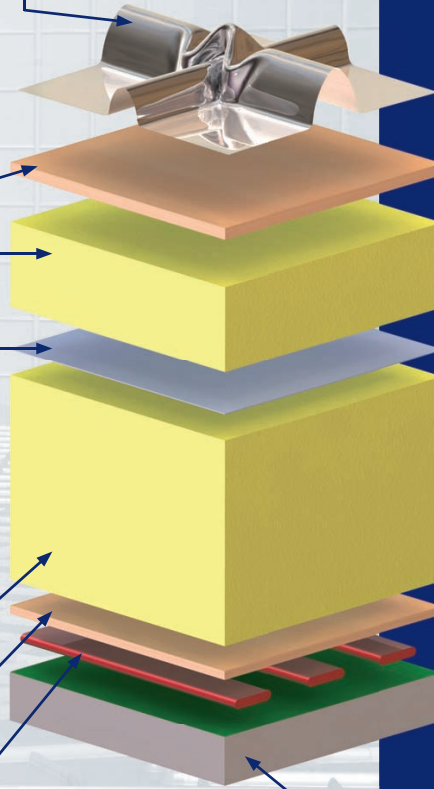


Figure 18: Exploded view of the membrane cryostat technology

**Insulation system and secondary membrane:** The membrane cryostat will have 0.9 m thick insulation panels applied to all internal surfaces (including the hatches) of the outer support structure and roof in order to control the heat ingress and hence required refrigeration heat load. The insulation material is a solid reinforced polyurethane foam manufactured as composite panels. The panels get laid out in a grid with 3 cm gaps between them (that will be filled with fiberglass) and fixed onto anchor bolts anchored to the support structure. The composite panels contain the two layers of insulation with the secondary barrier in between. After positioning adjacent composite panels and filling the 3-cm gap, the secondary membrane is spliced together by epoxying an additional overlapping layer of secondary membrane over the joint. All seams are covered so that the secondary membrane is a continuous liner.

In the GTT design, the secondary membrane is comprised of a thin aluminum sheet and fiberglass cloth. The fiberglass-aluminum-fiberglass composite is very durable and flexible with an overall thickness of about 1 mm. The secondary membrane is placed within the insulation space. It surrounds the bottom and sides. In the unlikely event of an internal leak from the primary membrane of the cryostat into the insulation space, it will prevent the liquid cryogen from migrating all the way through to the steel support structure where it would degrade the insulation thermal performance and could possibly cause excessive thermal stress in the support structure. The liquid cryogen, in case of leakage through the inner (primary) membrane will escape to the insulation volume, which is purged with GAr at the rate of one volume exchange per day.

**Outer support structure:** The proposed design is a steel support structure with a metal liner on the inside to isolate the insulation region and keep the moisture out. This choice allows natural and forced ventilation to maintain the temperature of the steel within its limit, without the need of heating elements and temperature sensors. The main body of the membrane cryostat does not have side openings for construction. The access is only from the top. There is a side penetration for the liquid argon pump for the purification of the cryogen.

**Top cap:** Several steel reinforced plates welded together constitute the top cap. The stainless steel primary membrane, intermediate insulation layers and vapor barrier continue across the top of the detector, providing a leak tight seal. The secondary barrier is not used nor required at the top. The cryostat roof is a removable steel truss structure that also supports the detector. Stiffened steel plates are welded to the underside of the truss to form a flat vapor barrier surface onto which the roof insulation attaches directly. The penetrations will be clustered in one region. The top cap will have two large openings for TPC installation, and a manhole to enter the tank after the hatches have been closed.

The truss structure rests on top of the supporting structure where a positive structural connection between the two is made to resist the upward force caused by the slightly pressurized argon in the ullage space. The hydrostatic load of the LAr in the cryostat is carried by the floor and the sidewalls. In order to meet the maximum deflection of 3 mm between APA and CPA and to decouple the detector from possible sources of vibrations, the TPCs will be connected to an external bridge over the top of the plate supported on the floor of the building. Everything else within the cryostat (electronics, sensors, cryogenic and gas plumbing connections) is supported by the steel plates under the truss structure. All piping and electrical penetration into the interior of the cryostat

are made through this top plate, primarily in the region of the penetrations to minimize the potential for leaks. Studs are welded to the underside of the top plate to bolt the insulation panels. Insulation plugs are inserted into the bolt-access holes after panels are mounted. The primary membrane panels are first tack-welded then fully welded to complete the inner cryostat volume. A list of the design parameters for the top of the cryostat can be found in the Appendix.

**Beam windows:** Multiple beam windows will be installed along the horizontal midplane on the upstream side of the LAr cryostat to allow particle beam to enter the active TPC volume with minimal energy loss and scattering. To simplify the mechanical design, we are exploring installing multiple modular beam windows as opposed to a single monolithic beam window. Each beam window will be identical in design and has a nominal circular cross section of about 20 cm in diameter. The window will be installed into a frame. The frame is assembled into the cryostat wall by the vendor at time of fabrication, and includes seals to both primary and secondary membranes. Inside the LAr volume, there will be low density "plugs" to displace the passive volume of LAr along the beam path length before the active TPC volume. The window design and configuration have not been finalized. There will likely be three or more beam windows installed on the cryostat to allow the beam to enter the cryostat at different locations and angles. Windows not being used for the active beam configuration will be covered by exterior flanges for safety.

**Cryostat grounding and isolation requirements:**

The cryostat has to be grounded and electrically isolated from the building. Figure 19 shows the layout of the top plate grounding. We list the grounding and isolation requirements for the cryostat.

**1. Isolation**

- (a) The cryostat membrane and the steel supporting structure shall be isolated from any building metal or building rebar with a DC impedance greater than 300 k $\Omega$ .
- (b) All conductive piping penetrations through the cryostat shall have dielectric breaks prior to entering the cryostat and the top plate.

**2. Grounding**

- (a) The cryostat, or "detector" ground, shall be separated from the "building" ground.
- (b) A safety ground network consisting of saturated inductors shall be used between detector ground and building ground.

**3. Top plate grounding**

- (a) The top grounding plate shall be electrically connected to the cryostat membrane by means of copper braid connections.
  - i. Each connection shall be at least 1.6 mm thick and 63.5 mm wide.
  - ii. The length of each connection is required to be as short as possible.

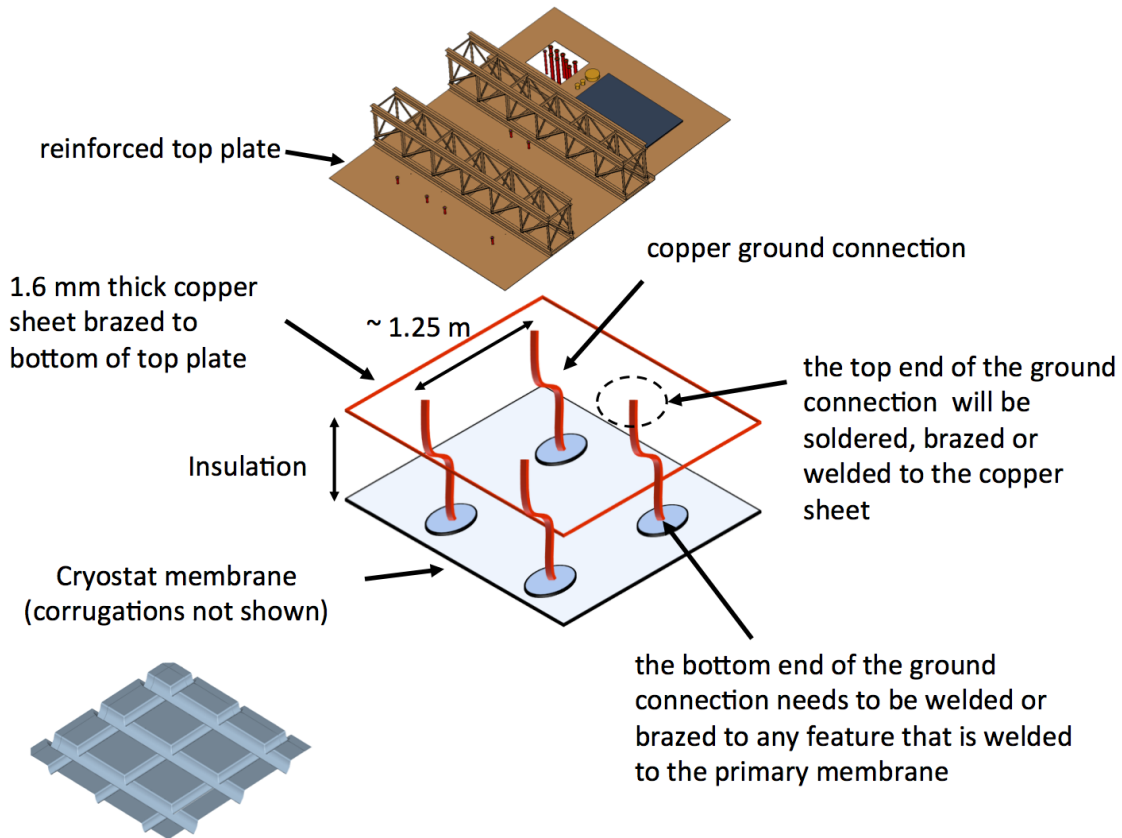


Figure 19: Top plate grounding layout

- iii. The distance between one connection and the next one shall be no more than 1.25 m.
- iv. The layout can follow the profile of several pieces of insulation, but it shall be continuous.
- v. The DC impedance of the membrane to the top plate shall be less than 1 ohm.

**Leakage quality assurance:** The primary membrane will be subjected to several leak tests and weld remediation, as necessary. All (100%) of the welds will be tested by an Ammonia colorimetric leak test (ASTM E1066-95) in which welds are painted with a reactive yellow paint before injecting a Nitrogen-Ammonia mixture into the insulation space of the tank. Wherever the paint turns purple or blue, a leak is present. The developer is removed, the weld fixed and the test is performed another time. Any and all leaks will be repaired. The test lasts a minimum of 20 hours and is sensitive enough to detect defects down to 0.003 mm in size and to a  $10^{-7}$  std-cm<sup>3</sup>/s leak rate (equivalent leak rate at standard pressure and temperature, 1 bar and 273 K). To prevent infiltration of water vapor or oxygen through microscopic membrane leaks (below detection level) the insulation spaces will be continuously purged with gaseous nitrogen to provide one volume exchange per day. The insulation space will be maintained at 70 mbar, slightly

above atmospheric pressure. This space will be monitored for changes that might indicate a leak from the primary membrane. Pressure control devices and safety relief valves will be installed on the insulation space to ensure that the pressure does not exceed the operating pressure inside the tank. The purge gas will be recirculated by a blower, purified, and reused as purge gas. The purge system is not safety-critical; an outage of the purge blower would have negligible impact on LAr purity.

## 4.2 Cryogenic system

Figure 20 outlines the basic scheme of the LN2 supply system, which was proposed by CERN for the Short Baseline Program and found to be an appropriate solution for this detector as well. The experiment will rely on LN2 tankers for regular deliveries to a

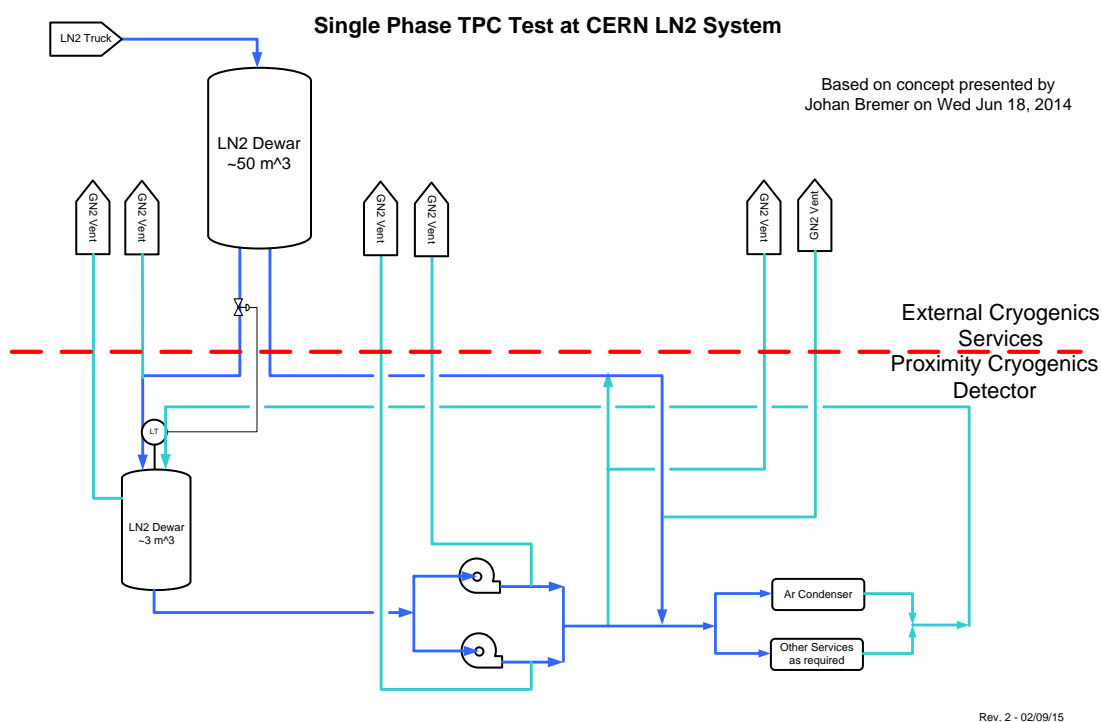


Figure 20: Schematic diagram for the proposed LN2 system

local dewar storage, which will be sized to provide several days of cooling capacity in the event of a delivery interruption. From the dewar storage the LN2 is then transferred to a distribution facility located in the experimental hall. It includes a small buffer volume and an LN2 pumping station that transfers the LN2 to the argon condenser and other services as needed. The low estimated heat leak of the vessel ( $\sim 3.2$  kW) and the location inside an above ground building allow for use of an open loop system typical of other installations operated at Fermilab (LAPD, 35 t prototype, MicroBooNE) and at CERN. The main goal of the LN2 system is to provide cooling power for the argon condenser, the initial cool down of the vessel and the detector, and all other services as needed. Table 3 presents the list of requirements for the DUNE-PT cryogenic system.

<b>Parameter</b>	<b>Value</b>
Location	Preferably not in front of the cryostat (on the beam)
Cooling Power	TBD based on the heat leak of the cryostat (estimated 3.4 kW), the cryo-piping and all other contributions (cryogenic pumps, etc.)
Liquid argon purity in cryostat	10 ms electron lifetime (30 ppt O <sub>2</sub> equivalent)
Gaseous argon piston purge rate of rise	1.2 m/hr
Membrane cool-down rate	From manufacturer
TPCs cool-down rate	<40 K/hr, <10 K/m (vertically)
Mechanical load on TPC	The LAr or the gas pressure shall not apply a mechanical load to the TPC greater than 200 Pascal.
Nominal LAr purification flow rate (filling/ops)	5.5 day/volume exchange
Temperature of all surfaces in the ullage during operations	<100 K
Gaseous argon purge within insulation	1 volume change /day of the open space between insulation panels.
Lifetime of the cryogenic system	Consistent with the LAr program. TBD.

Table 3: Design requirements for the cryogenic system

### Single Phase TPC Test at CERN LAr Systems

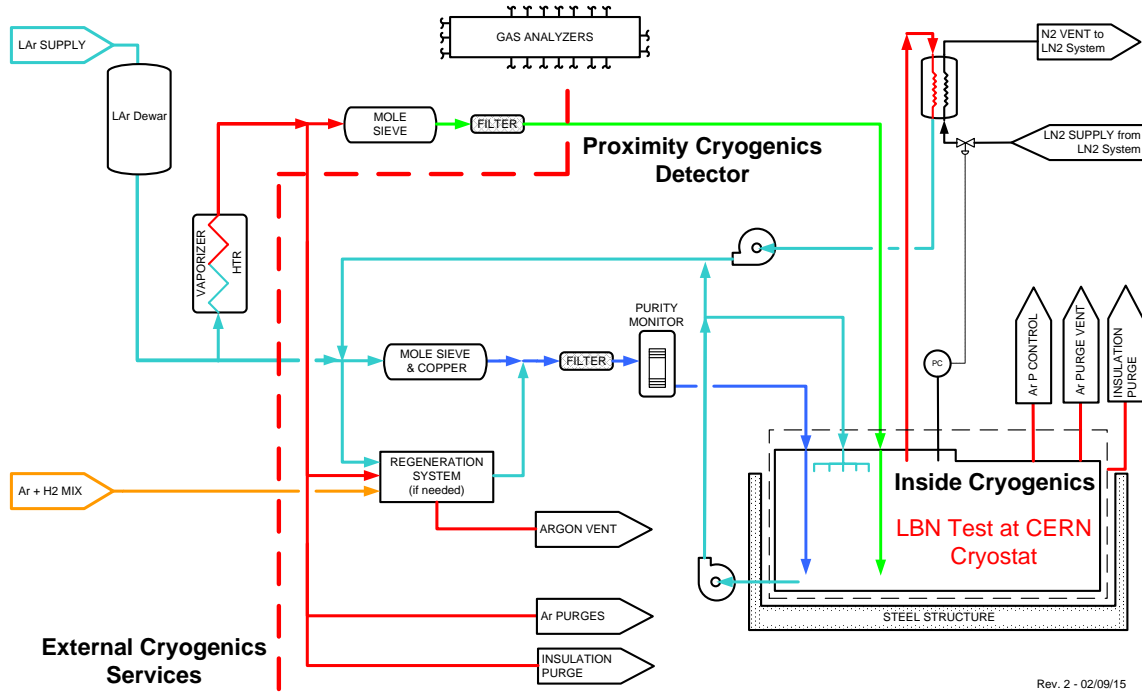


Figure 21: Schematic diagram for the proposed LAr system

Figure 21 shows a schematic diagram of the proposed liquid argon system. It is based on the design of the 35 t prototype, the MicroBooNE detector systems and the plans for the DUNE Far Detector. The main goal of the LAr system is to purge the cryostat prior to the start of the operations (with GAR in open and closed loop), cool down the cryostat and fill it with LAr. The next step is to continuously purify the LAr and the boil off GAR to maintain the required purity which is measured by the detector in the form of an electron drift time measurement.

The LAr receiving facility includes a storage dewar and an ambient vaporizer to deliver LAr and GAR to the cryostat. The LAr goes through the liquid argon handling and purification system, whereas the GAR through the gaseous argon purification before entering the vessel.

The LAr purification system is currently equipped with a filter containing mol sieve and copper beads, and a regeneration loop to regenerate the filter itself. Filters containing Oxsorb and Hydrosorb rather than mol sieve and copper beads represent a proven alternate solutions. Studies are ongoing to standardize the filtration scheme and select the optimal filter medium for all future generation detectors, including the CERN prototypes.

During operation, an external LAr pump circulates the bulk of the cryogen through the LAr purification system. The boil off gas is first recondensed and then is sent to the LAr purification system before re-entering the vessel.

## 5 Calibration

The design of the calibration system for DUNE-PT pursues two principal goals. The first is to calibrate the detector itself to provide high quality data for successive data analysis and the second is to test and optimize the calibration tools themselves for future use in the DUNE far detectors.

The accuracy of track and kinematics reconstruction and particle identification largely relies on the knowledge of the electric field map, purity map, and temperature inside the active detector volume. The electric field in the drift region, designed to be a uniform 500 V/cm, could vary at different locations due to sagged wires, misalignment and imperfections in the field cage.

The electric field could also be distorted by the space charge. Electrons and ions which are generated by the passing of high energy particles drift in opposite directions to anode and cathode planes, respectively. The electrons drift at about 1.6 mm/ $\mu$ s and take 2.25 ms to travel the maximum distance between APAs and CPAs. The ions, drifting at  $\sim 8 \times 10^{-6}$  mm/ $\mu$ s, can take up to 7.5 minutes to travel the same distance. The surface cosmic ray flux entering the detector imposes a large space-charge effect to the detector. Distortion of the electric field could result in centimeter levels of uncertainty in position reconstruction and can also make a difference in electron-ion recombination and light output.

The temperature of liquid argon affects the electron drift velocity and has a gradient of about -1.9%/K. Precision measurement of temperature could be easily achieved with commercial silicon diode sensors down to tens of milliKelvin.

Purity of argon directly affects the amount of surviving electrons, which would be used to estimate the amount of energy deposited in that wire space. This energy deposition, dE/dx, is a key quantity for particle identification. Monitoring argon purity is also essential for the operation of the experiment.

Multiple means should be employed to measure the electric field, the purity of liquid argon and its temperature. The presently foreseen calibration equipment includes:

- Gas purity analyzers
- Liquid purity monitors
- Temperature sensors
- Laser calibration system
- Muon detector system

The gas purity analyzers for oxygen and H<sub>2</sub>O are commercially available. These analyzers measure purity down to a few parts per billion (ppb). They are not directly measuring the liquid argon purity in the detector but can be installed outside of the detector and take samples from various points of the cryogenic system and thereby provide an overview of the detector system.

Liquid purity monitors are small size TPCs with light sources that generate electrons via photoelectric effect and electronics to read out the amount of electrons in the cathode plane and anode plane. The electron lifetime can be derived by comparing the number

of surviving electrons with those generated. The electron lifetime is a direct estimator of the argon purity. Multiple liquid purity monitors will be installed at a variety of locations (close to and far from the recirculation inlet) and at different heights.

The temperature of liquid argon varies as a function of the pressure of the detector by a little less than 1 K/psi. Silicon diode sensors with accuracy as little as  $\sim 20$  mK will be installed at multiple locations in the detector.

To measure and calibrate electric field, purity, electron lifetime and drift speed in-situ, a laser system and a muon detector are foreseen. Both systems, each with particular pros and cons, use ionization-particle paths to measure the above quantities.

The **laser calibration system** employs a high power ultra-violet (UV) laser to ionize the liquid argon. The 266 nm UV photons have energy of 4.66 eV. Three photons could ionize one argon molecule (ionization potential for liquid argon is 13.78 eV). A laser beam is directed into the TPC region via a steerable feedthrough, which allows reflection of the laser beam to various regions of the active detector volume. The laser energy is about 10 mJ, which corresponds to  $10^{16}$  UV photons, and has sufficient energy to produce a straight (long Rayleigh scattering length) and uniform ionization path. Due to the size of the laser beam, about 1 cm in diameter, the electrons are generated in a relatively large space, and the electron-ion recombination effect is negligible compared to the cosmic ray induced ionization. In the proposed TPC configuration with a CPA in the center and two APAs on the outsides, the laser feedthrough will be installed outside of the TPC region and in the same plane as the central CPA. Therefore the laser beam can be directed to both CPA-APA regions. The field cage is designed with multiple slits to allow the laser beam to pass to the inside of the TPC. Position detection systems such as SiPMs will be installed on the other side of the field cage to measure the position of the laser beam.

The **cosmic muon detector** system serves as an alternative tool to the laser calibration system. Cosmic rays with energies of a few GeV have nearly uniform  $dE/dx$  in liquid argon with about 2 MeV/cm and generate about 18,000 electrons/cm. Given standard values quoted for the cosmic ray muon flux at sea level, we arrive at a number of roughly 200 incident muons per square meters per second. Taking into account the dimensions of the TPC, we estimate the area of the top face of its rectangular volume to be just over 50 m<sup>2</sup>, which means that the detector will be subject to  $\sim 10^4$  particles per second. The full electron drift time in liquid argon for a 3.6 m drift length is 2.25 ms, and each readout window for an event will contain three drift time windows which will include data from drift windows before and after the event. Based on the cosmic rate and the size of the readout window, there is expected to be on average  $\sim 68$  track segments on top of the actual beam event. This estimate takes into account the readout of charge that may still be drifting from the window just prior to the triggered one and the loss of charge that is still drifting after the triggered window ends. Muon detectors are planned to be installed to preferentially measure cosmic rays passing nearly horizontally through the cryostat. Additional muon counters on top of the cryostat will allow tagging of highly inclined muons and veto of vertical muons. A disadvantage of using muons as a calibration tool compared to a laser beam is that muons could scatter multiple times in passing through more than 7 meters of liquid argon and will therefore not be perfectly straight anymore.

## 6 Charged Particle Test Beam Requirements

### 6.1 Particle beam requirements

The requested beam parameters are driven by the requirement that the results from the CERN test beam should be directly applicable to the future large underground single-phase LAr detector with minimal extrapolation. The CERN test beam data will be used to evaluate the detector performance, to understand the various physics systematic effects, and to provide “neutrino-like” data for event reconstruction studies. To satisfy the requirement, the beam parameters must span a broad range of particle spectrum that are expected in the future neutrino experiment. The particle beam composition should consist of electrons, muons, and hadron beams that are charge-selected. The expected momentum distributions for secondary particles from neutrino interactions are shown in Figure 3. There is a large spread in the momentum distribution with most particles peaked near 200 MeV/c. To cover the momentum range of interest, the momentum of the test beam should step from 0.2 GeV/c up to 10 GeV/c.

The maximum electron drift time in the TPC is about 2.2 ms. In order to minimize pile-up in the TPC, the planned beam rate should be around 200 Hz. The DUNE-PT has two drift volumes separated by a passive cathode plane. It is desirable to aim the particle beam such that a large fraction of the lower energy hadronic showers are mostly contained in one drift volume to minimize uncertainties due to the passing of inactive detector materials.

The nominal plan is to have the beam enter the cryostat slightly downward at an angle of about 6 degrees. This angle will roughly match the angle at which the neutrino beam enters the liquid argon cryostat at the far detector for the DUNE experiment. Along the horizontal plane, the beam should enter the cryostat with an angle of about 10 degrees to avoid pointing the beam perpendicular to the electron drift in the TPC. Events with the latter orientation would introduce larger reconstruction ambiguities. We also plan to take some data with the beam entering a different region of the TPC, and may include some data with particles crossing one drift volume to the next. The summary of the beam requirements are shown in Table 4.

### 6.2 EHN1 H4ext beamline and beam instrumentation

The H4ext is an extension of the existing H4 beamline in Experimental Hall North 1 (EHN1). To produce particles in the momentum range of interest, a 60-80 GeV/c pion beam from the T2 target is used to generate tertiary beams. The tertiary particles are momentum and charge-selected and transported down H4ext beamline to the experimental area. A conceptual layout of the H4ext beamline is shown in Fig. 22. The top plot in Fig. 22 is the bird’s eye view and the bottom plot is the side view of the beam line layout.

Beam instrumentation provides important information about the characteristics of the beam. It is expected that a series of detectors will be installed along the beam line to measure the particle momentum, identify particle type, and track the particle trajectory.

Parameter	Requirements
Particle Types	$e^\pm, \mu^\pm, \pi^\pm, K, p$
Momentum Range	0.2 - 10 GeV/c
Momentum Spread	$\Delta p/p < 5\%$ (limited by the aperture of the magnets)
Transverse Beam Size	RMS(x,y) $\approx 10$ cm (At the entrance face of the LAr cryostat)
Beam Divergence	tbd
Beam Angle (horizontal plane)	$\approx 10^\circ$ (w.r.t. the long axis of the cryostat)
Beam Dip Angle (vertical plane)	$\approx 6^\circ$ (downward from horizontal)
Beam Entrance Position	Multiple beam windows
Rates	200 Hz (maximum)

Table 4: Particle beam requirements.

### 6.2.1 Beam position detector

The beam position detector measures the positions of the particle as it traverses the detector. Two detector technologies are under considerations: wire chambers and scintillating fiber trackers. For the nominal setup, one beam position detector is installed upstream and another one downstream of the last bending magnet. This pair provides additional momentum information about the particles as well as the first set of position measurements. Without tracking information, the momentum spread of the beam is expected to be at around 5% based on the acceptance of the dipole magnets. With additional tracking information, we are likely to be able to measure the momentum of the individual particles to close to one percent level. A third beam position detector is placed right in front of the beam window on the cryostat wall to provide the last position information before the beam enters the cryostat.

### 6.2.2 Particle identification

In order to have good particle identification over large momentum range, two independent particle identification systems are needed in the beamline. The Time-of-Flight system will be used to cover the lower momentum range while a Threshold Cherenkov detector will be tuned for higher momentum particles. We will require  $\geq 3\sigma$   $K/\pi$  separation for momentum range from 0.2 to a few GeV/c. Work is in progress to better define the beamline layout to meet the requirements.

### 6.2.3 Muon beam halo counters

The muon beam halo counters is a set of detectors (e.g. plastic scintillator paddles) surrounding the beamline. The main purpose is to tag particles (primarily muons from the upstream production target) that are outside of the beam axis, but may potentially enter the TPC volume. The counter information is used to either veto or simply flag

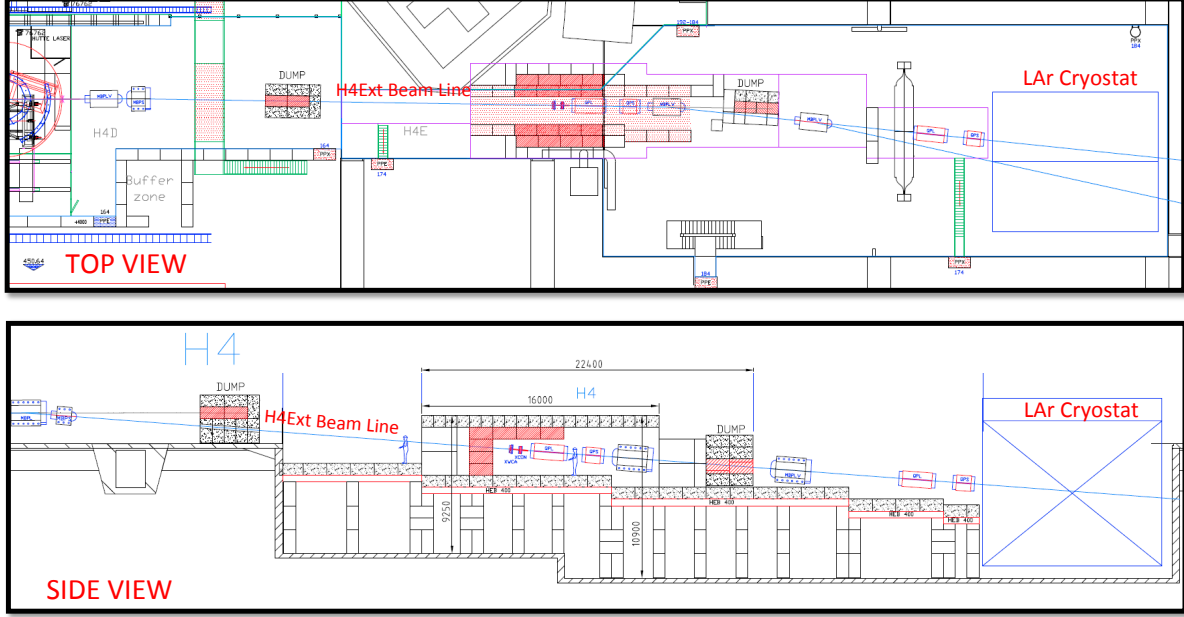


Figure 22: A conceptual layout of the H4ext beamline. The top plot is the bird's eye view and the bottom plot is the side view of the H4ext beam line in EHN1. The liquid argon cryostat for this proposal is the rectangular box in the right hand corner of both plots. The beam nominally enters the TPC at an angle of about  $10^\circ$  horizontally (top plot). On the vertical plane (bottom plot), the beam enters the cryostat downward with an angle of about  $6^\circ$ . Multiple beam windows will be installed on the upstream wall of the cryostat to allow the beam to enter the TPC from different positions and angles.

these class of events. The Muon Beam Halo counter can be a subset of the cosmic muon veto system.

### 6.3 Beam rates and run plan

At the time of this proposal, the beamline design has not been finalized. To estimate the beam rates, we use inputs from a generic target simulation based on 100k 80 GeV  $\pi^+$  beam on 15 cm copper target. This  $\pi^+$  rate is roughly equivalent to 10% of a typical SPS spill. The distributions of the tertiary particles from the copper target are shown in Fig. 23. The figure on the left is for postively charged and the figure on the right is for negatively charged tertiary particles.

To formulate a preliminary beam time request, we assume the hadron beam rates and spectrum as given in Fig. 23. For the beam rate estimates, we account for particle decays assuming the distance from the secondary target to the cryostat to be 30 m. A significant fraction of pions and kaons below 1 GeV/c decay before reaching the liquid argon cryostat. In addition, we also assume the data taking efficiency to be about 50%. For the electron sample, we expect a different optimized beamline setup to produce a pure electron beam with a flux of about 200 Hz. A preliminary run plan for one configuration is shown in Table 5. The number of spills needed for each momentum bin is driven by the samples highlighted in red. The minimum beam time requirement is 150 spills ( $\approx$  2 hours of beam time) per momentum bin to ensure we have sufficient data taken with

Positive Sample						
$P$ (GeV)	# of Spills	Time (hours)	# of $\pi^+$	# of $\mu^+$	# of $K^+$	# of p
0.2	900	11	<b>15k</b>	180k	$\approx 0$	160k
0.3	200	3	<b>15k</b>	30k	$\approx 0$	50k
0.4	150	<b>2</b>	22k	18k	$\approx 0$	32k
0.5	150	<b>2</b>	26k	12k	$\approx 0$	38k
0.7	150	<b>2</b>	40k	10k	$\approx 0$	45k
1	350	4	120k	<b>10k</b>	$\approx 0$	65k
2	600	8	320k	<b>10k</b>	3k	130k
3	500	6	290k	<b>5k</b>	7k	70k
5	1800	23	1M	<b>5k</b>	5k	270k
7	1200	15	660k	<b>6k</b>	3k	120k
Total	6000	76	2.5M	286k	18k	1M
Negative Sample						
$P$ (GeV)	# of Spills	Time (hours)	# of $\pi^-$	# of $\mu^-$		
0.2	600	8	<b>15k</b>	88k		
0.3	200	3	<b>15k</b>	30k		
0.4	150	<b>2</b>	30k	18k		
0.5	150	<b>2</b>	40k	13k		
0.7	150	<b>2</b>	50k	12k		
1	150	<b>2</b>	70k	12k		
2	200	3	135k	<b>6k</b>		
Total	1600	22	350k	180k		
Electron Sample						
$P$ (GeV)			# of Spills	Time (hours)	# of electron	
0.2,0.3,0.4,0.5,0.7,1,2,3,5,7			150 per bin	2 hours per bin	140k per bin	
Total			1500	20	1.4M	

Table 5: A preliminary run plan for one beam angle and position. The number of spills needed for a given momentum bin is driven by the samples highlighted in red or by the requirement of at least 150 spills per momentum bin.

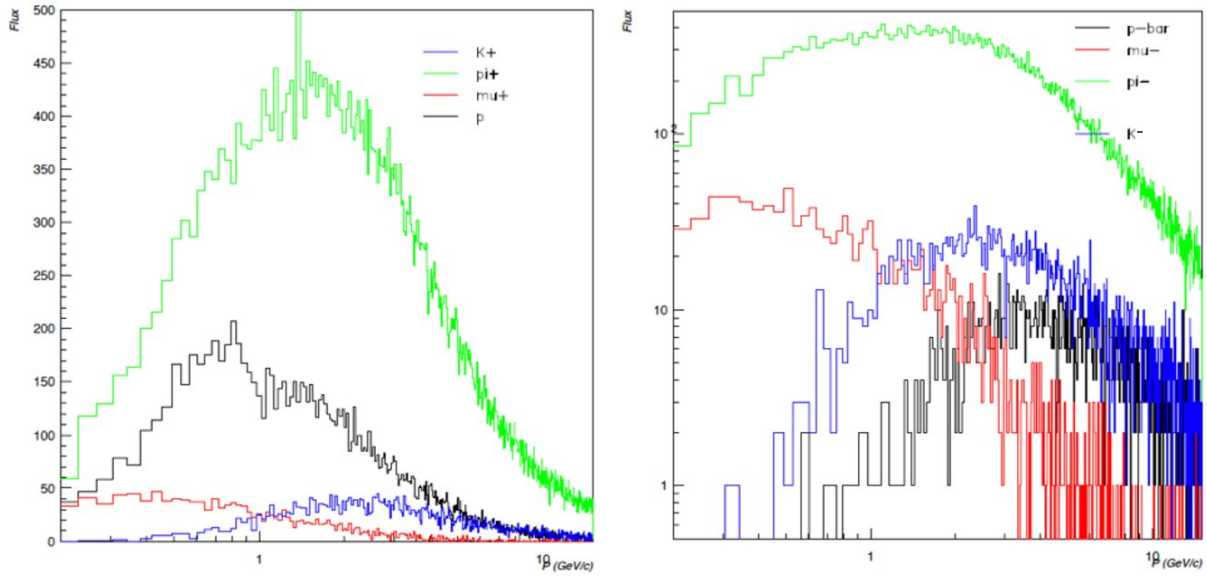


Figure 23: Simulated flux of charged secondary particles resulting from 100k  $\pi^+$  each with an energy of 80 GeV impinging on a 15 cm copper target. The figure on the left is for positively charged and the figure on the right is for negatively charged secondary particles.

stable beam running. This proposed plan satisfies the requested samples as listed in Table 1, except for kaons less than 1 GeV. Most low momentum kaons produced from the secondary target decay before reaching the liquid argon cryostat. To obtain those samples, we will need to carry out extended runs and trigger exclusively on particles tagged as kaons by either the time-of-flight or the threshold Cherenkov counters.

In addition to the above samples with beam at the nominal position, we expect to take some additional data with the beam entering the TPC at different position and angles. Without a detail beamline design, there are still some uncertainties on the actual beam rates. We are working on estimating the amount of beam time required. Based on the current information that we have, the total estimated beam time needed to carry out the physics program (physics samples as listed in Table 1, multiple angles and beam positions, dedicated kaon runs, etc) in this proposal is in the range of 4 to 6 weeks.

## 7 Computing, Data Handling and Software

DUNE-PT builds upon the technology and expertise developed in the process of design and operation of its smaller predecessor, the 35 t detector at Fermilab. This includes elements of front-end electronics, data acquisition, run controls and related systems. We also expect that for the most part, Monte Carlo studies necessary to support this program will be conducted using software evolved from current (2015) tools. Likewise, event reconstruction software and analysis tools will rely on the evolving software tools developed for DUNE.

The volume of the recorded data will depend on the number of events to be collected

in each measurement, as specified in the run plan (see Table 5). Cosmic ray muons have a very large impact on the data volume due to the large detector dimensions and surface operation.

It is optimal to first stage the data collected from DUNE-PT on disk at CERN and then save it to tape also at CERN, while simultaneously performing replication to data centers in the US. For the latter, Fermilab will be the primary site, with additional data centers at Brookhaven National Laboratory (BNL) and the National Energy Research Scientific Computing Center (NERSC) facility as useful additional locations for better redundancy and more efficient access to the data from a greater number of locations.

## 7.1 Event size estimate and data volume

The data volume will be dominated by the TPC data. Even though the photon detector as well as other elements of the experimental apparatus (muon counters, trigger systems) contribute to the data stream their contributions to the data volume are expected to be sufficiently small such that realistic data volume estimates can be obtained from the TPC event data sizes alone.

Event sizes can be estimated from "first principles" under the assumption of some event topology and noting the significant amount of cosmic contamination at sea level. As was shown in Sec. 5, there is expected to be on average  $\sim 68$  cosmic muon track segments per readout window and on top of the actual beam event. Given that a 4 GeV Minimum Ionizing Particle (MIP) will produce on average 80 kbyte of data, the resulting number of particles in a readout window will result in the readout of 6 MB per beam event. In addition to the data associated with the individual particles in the event, channel overhead information needs to be accounted for. Experience from the 35 t detector at Fermilab indicates that with zero suppression the event overhead amounts to 6 kB per channel for a readout of three drift windows. Since there are 15,360 channels in DUNE-PT, the expected overhead corresponds to 92 MB per event. The resulting total event size from overhead and charge from individual particles is 100 MB.

The total particle statistics in the preliminary run plan (Table 5) is approximately 5M events in total. Taking into account the data load per event, this leads to the estimate of  $\sim 500$  TB of nominal data volume to be collected in this experiment.

In summary, we expect that tape storage of  $O(1\text{PB})$  size will be required and a somewhat more modest disk space for raw data staging at CERN, for replication purposes. We envisage storing the primary copy of raw data at CERN, with replicas at additional locations. Processed and Monte Carlo data placement will require additional resources that are addressed in Section 7.3.1.

### 7.1.1 Data transmission and distribution

Moving data to remote locations outside of CERN is subject to a number of requirements that include automation, monitoring and error checking and recovery.

A number of candidate systems satisfy these requirements and we would like to explore CERN based options and take advantage of local know-how. An alternative for which we have expertise and experience is Spade, which was first used in IceCube [38] and then enhanced and successfully utilized in the Daya Bay experiment [39].

## 7.2 Databases

Databases will be required to store Run Logs, Slow Control records and detector conditions, as well as (offline) calibration information.

Most database servers will need to be local to the experiment (i.e. at CERN) in order to reduce latency, guarantee reliability and minimize downtime due to network outages. A replication mechanism is foreseen to make data readily available at the US and other sites. The volume of data stored in these databases is expected to be modest and of the order of 100 GB.

## 7.3 Computing and software

Fermilab provides the bulk of computational power to DUNE via Fermigrid and other facilities. We plan to leverage these resources to process the data coming from the DUNE-PT and beam test.

One of the principal goals will be quick validation of the data collected in each measurement, in order to be able to make adjustments during the run as necessary. This is common practice in other experiments which have "express streams" to assess data quality [40].

Given that tracking, reconstruction and other algorithms are in a stage of development with significant improvements and optimizations expected, the required scale of CPU power needed to process the data are rough estimates. The estimates we have at this point range from 10 to 100 seconds required by a typical CPU to reconstruct a single event. This means that utilizing a few thousand cores through Grid facilities, it will be possible to ensure timely processing of these data.

To ensure adequate capacity, we envisage a distributed computing model where Grid resources are utilized in addition to Fermilab's computing resources. As an example, we have had good experience working with the Open Science Grid Consortium.

### 7.3.1 Data processing

In addition to the raw data preparations being made for offline data handling, processing and storage. The offline data can be classified as follows:

- Monte Carlo data, which will contain multiple event samples to cover various event types and other conditions during the measurements with DUNE-PT
- Data derived from Monte Carlo events, and produced with a variety of tracking and pattern recognition algorithms in order to create a basis for the detector characterization
- Intermediate calibration files, derived from calibration data
- Processed experimental data, which will likely exist in several parallel branches corresponding to different reconstruction algorithms being applied, with the purpose of evaluating the performance of the different algorithms.

In the latter, there will likely be more than one processing step, thus multiplying data volume.

The derived data will at most contain a small fraction of the raw data in order to keep the data manageable. Hence the size of the processed data will likely be significantly smaller than the input (the raw data). Given the consideration presented above, we will plan for  $\sim O(1 \text{ PB})$  of tape storage to keep the processed data. For efficient processing, disk storage will be necessary to stage a considerable portion of both raw data (inputs) and one or a few steps in processing (outputs).

Extrapolating from our previous experience running Monte Carlo for the former LBNE Far Detector, we estimate that we will need a few hundred TB of continuously available disk space. In summary, we expect the need for a few PB of disk storage at Fermilab to ensure optimal data availability and processing efficiency.

### 7.3.2 Data distribution

We foresee that data analysis (both experimental data and Monte Carlo) will be performed by collaborators residing in many institutions and geographically dispersed. In our estimate above, we mostly outlined storage space requirements for major data centers like CERN and Fermilab. When it comes to making these data available to collaborators, we will utilize a combination of the following:

- Managed replication of data in bulk, performed with tools like Spade. Copies will be made according to wishes and capabilities of participating institutions.
- Network-centric federated storage, based on XRootD. This allows for agile, just-in-time delivery of data to worker nodes and workstations over the network. This technology has been evolving rapidly in the past few years, and solutions have been found to mitigate performance drops due to remote data access, by implementing caching and other techniques.

In order to act on the latter item, we plan to implement a global XRootD redirector, which will make it possible to transparently access data from anywhere. A concrete technical feature of storage at Fermilab is the dCache network which has substantial capacity and can be leveraged for the needs of the DUNE-PT data analysis. This dCache instance is equipped with a XRootD “door” which makes it accessible to the outside world, subject to proper configuration, authentication and authorization.

Copies for a significant portion of raw and derived data are planned to be hosted at NERSC and also at Brookhaven National Laboratory. These two institutions have substantial expertise in the field of data handling and processing at scale and will serve as “hubs” for data archival and distribution.

### 7.3.3 Software infrastructure

The DUNE-PT effort will benefit from utilizing simulation toolkits, tracking and other reconstruction that have and continue to be developed for DUNE, the 35 t detector and the short baseline program at Fermilab as well as the neutrino platform development efforts and in particular the WA105 experiment.

The software tools will need to be portable, well maintained and validated. To ensure that this happens, we plan to establish close cooperation among participating laboratories and other research institutions.

## 8 Installation and Infrastructure

### 8.1 Installation

The outer steel support structure for the cryostat will be prefabricated in pieces of dimensions appropriate for transportation, shipped to the destination and only assembled in place. Fabrication will take place at the vendor's facility for the most part. This shortens the construction of the outer structure on the detector site, leaving more time for completion of the building infrastructure. If properly designed, a steel structure may allow the cryostat to be moved, should that be desired in the future.

The TPC and PDS detector components will be manufactured and submitted to quality assurance procedures at one or more of the potential DUNE detector component production sites. Successively, components will be shipped to CERN for further testing and final assembly into the cryostat. This approach will begin the preparations for the various production sites for the first 10 kt module of the DUNE far detector.

The interior of the cryostat will be prepared prior to the installation of the TPC. Several I-beam support rails will be suspended below the top surface of the cryostat membrane by a series of hangers. These hangers will be supported by an independent structure above the cryostat. Decoupling the TPC support from the cryostat structure eliminates the movement of the TPC with the flexure of the cryostat structure from the filling and internal pressure changes of the Argon inside. The hangers will pass through the top of the cryostat to the independent structure inside a bellows type feedthrough. These feedthroughs need to be designed to minimize the heat flow into the cryogenic volume. For the CPAs, the support rails and hangers need to be electrically isolated due to high voltage concerns.

There will be a series of feedthrough flanges located along each of the support rails. These will be cryogenic flanges where the services for the TPC components can pass through the top of the cryostat. It is foreseen that the CPA row will require one feedthrough for the high voltage probe to bring in the drift voltage. The drift field is 500 V/cm. For a drift distance of 3.6 m and 2.5 m, the probe voltages will be 180 kV and 125 kV, respectively. There will be one service feedthrough for each of the APAs. These feedthroughs will include high speed data connections, bias voltages for the wire planes, control and power for the cold electronics.

The main TPC components will be installed through large hatches in the top of the cryostat. This is similar to the installation method intended for the detector at the DUNE far site. These hatches will have an aperture approximately 2.0 m wide and 3.5 m long. Each APA and CPA panel will be carefully tested after transport into the clean area and before installation into the cryostat. Immediately after a panel is installed it will be rechecked. The serial installation of the APAs along the rails means that removing and replacing one of the early panels in the row after others are installed would be very costly in effort and time. Therefore, to minimize the risk of damage, as much work around already installed panels as possible will be completed before proceeding with further panels.

In general, APA panels will be installed in order starting with the panel furthest from the hatch side of the cryostat and progressing back towards the hatch. The upper field cage will be installed in stages as the installation of APAs and CPA panels progresses.

After the APAs are attached to the support rods the electrical connections will be made to electrical cables that were already dressed to the support beams and electrical testing will begin. Periodic electrical testing will continue to assure that nothing gets damaged during the additional work around the installed APAs.

The TPC installation will be performed in three stages, each in a separate location. First, in the clean room vestibule, a crew will move the APA and CPA panels from storage racks, rotate to the vertical position and move them into the cryostat. Secondly, in the panel-staging area immediately below the equipment hatch of the cryostat, a second crew will transfer the panels from the crane to the staging platform, where the crew inside the cryostat will connect the panels to the rails within the cryostat. A third crew will reposition the movable scaffolding and use the scaffold to make the mechanical and electrical connections at the top for each APA and CPA once they are moved into position.

The requirements for alignment and survey of the TPC are under development. Since there are many cosmic rays in this detector due to its location on the surface, significant corrections can be made for any misalignments of the TPC. The current plan includes using a laser guide or optical transit and the adjustment features of the support rods for the TPC to align the top edges of the APAs in the TPC to be straight, level and parallel within a few millimeters. The alignment of the TPC in other dimensions will depend on the internal connecting features of the TPC. The timing of the survey will depend on understanding when during the installation process the hanging TPC elements are in a dimensionally stable state. The required accuracy of the survey is not expected to be more precise than a few millimeters.

## 8.2 Infrastructure

The inner detector and surrounding cryostat of DUNE-PT will be located in a recessed pit in the floor of the extension of the EHN1 experimental hall. However, additional space will be required for the installation and operation of DUNE-PT. This includes an unloading area, a clean room for assembly, and a control room to host computers to operate the detector components, readout the detector, and provide local storage of detector data. Crane and forklift access will be required in the unloading zone and crane transport of detector components will be required between the clean room and recessed pit. The control room will have to be accessible 24 hours a day and 7 days a week.

The experiment will rely on liquid nitrogen to provide cooling power for the argon condenser and the initial cool down of the vessel and the detector. The area will have to be setup to receive regular tanker deliveries to a local dewar storage. A distribution facility located in the experimental hall will be used to transfer the liquid nitrogen from the dewar system. In addition, a liquid argon receiving facility which includes a storage dewar and an ambient vaporizer will be used to deliver liquid argon and gaseous argon to the cryostat. Because of the risk of argon collecting in the pit, an exhaust pipe out of the pit will be required to vent the area. The humidity and temperature in the experimental area will need to be controlled by air conditioning.

The experimental hall will need to supply dedicated electrical power for the various components. These include: the cryogenic system (*e.g.* pumps), front-end electronics, high voltage systems, monitor systems, computers, etc.

## 9 Schedule, Organization and Cost Estimate

### 9.1 Organization

Construction and operation of the DUNE-PT is an integrated effort within the experimental program of the DUNE collaboration. The DUNE Collaboration management team includes the collaboration Co-Spokespersons, Andre Rubbia (ETH Zurich) and Mark Thomson (Cambridge University); the Technical Coordinator, Eric James (Fermilab); and the Resource Coordinator, Chang Kee Jung (Stony Brook University). This team is responsible for coordinating the international effort required to design, construct, install, commission, and operate the detectors needed to achieve the scientific objectives of the DUNE Collaboration.

The DUNE-PT is an integral part of this effort. This detector will be built from full-scale components and designed to replicate the configuration of the first 10 kt detector module to be installed at the Sanford Underground Research Facility (SURF) in South Dakota during the early 2020s. Successful construction and operation of the DUNE-PT will validate the design of this much larger detector, and the accomplishment of these tasks is among the highest priorities for the DUNE Collaboration over the timescale of the next few years. Additionally, the subsequent collection and analysis of test beam data from the DUNE-PT will provide vital calibration data necessary to achieve DUNE's scientific goals.

In addition to taking responsibility for the construction and operation of the DUNE-PT, the DUNE collaboration strongly endorses the already approved dual-phase liquid argon detector development program at CERN (WA105 experiment), recognizing the potential advantages of this detector technology, which may ultimately be chosen for one or more of the three additional 10 kt detector modules to be installed at SURF.

The organization of the DUNE collaboration is shown in Fig. 24. The international DUNE Project Office is overseen by the Technical Coordinator and coordinates the work packages assigned to each of the different international partners contributing to the effort. The Project Office maintains a schedule covering the entire scope of the project (incorporating all of the individual work packages) and tracks progress through a detailed set of milestones embedded within this schedule. The schedule is based on a Work Breakdown Structure (WBS), which within its cascading levels incorporates all required components of the detector construction projects. The highest-level elements within this WBS encompass multiple work packages assigned to different international partners. The deliverables associated with individual work packages become separated at lower levels within the WBS, where the contributions from specific partners are broken out as independent WBS elements.

The DUNE Collaboration structure incorporates detector and prototyping organizations that mimic the WBS of the project. All matters related to the design, construction, installation, and commissioning of individual detector elements are discussed within these organizations. Because these organizations serve as the required interface between the DUNE Collaboration and the international DUNE Project, they incorporate both a coordinator who reports to the DUNE Executive Committee through the Technical Board of the collaboration and a manager who reports to the Project Office. The coordinators and managers of the organizations are also members of the Technical

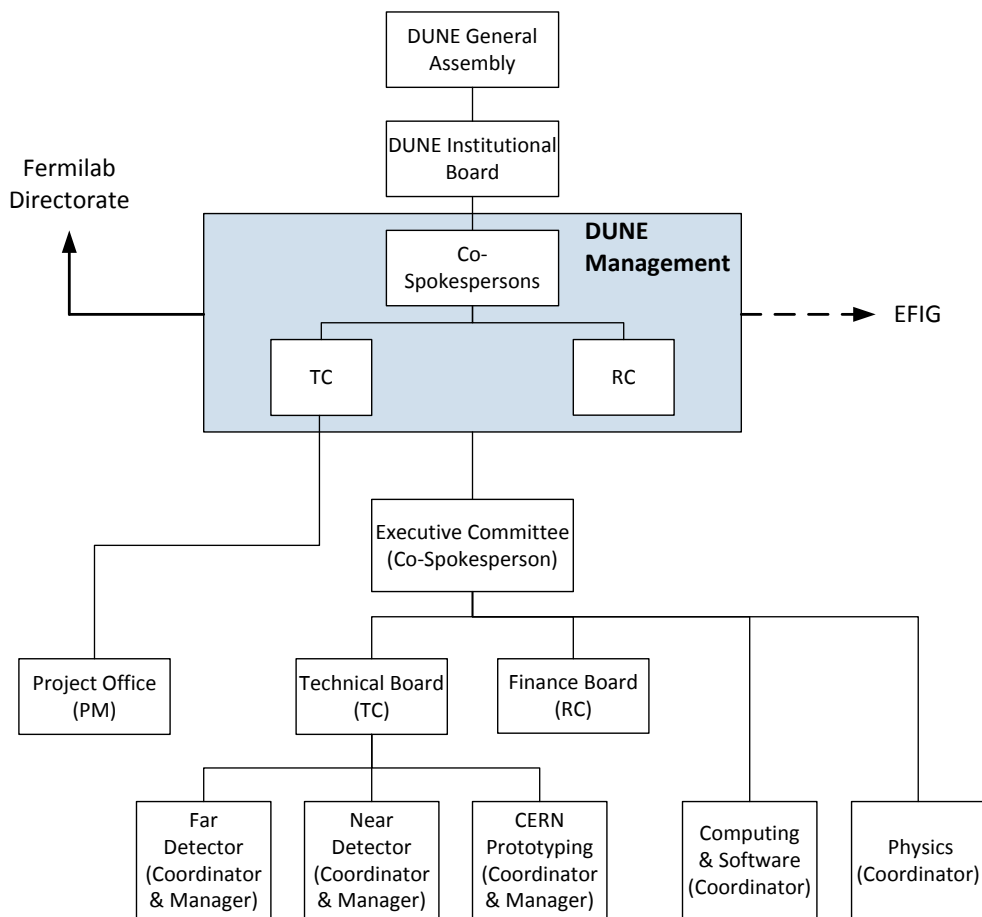


Figure 24: Organization of the DUNE collaboration.

Board, which coordinates activities across organizations and acts on lower-level project change control requests. Coordination of simulation and data analysis activities are the responsibilities of the Computing & Software and Physics Coordinators, respectively, who report directly to the collaboration Executive Committee and manage collaboration working groups covering the full scope of activities within their areas.

As shown in Fig. 24, the collaboration structure includes a high-level organization focusing specifically on the CERN prototyping effort. The interim coordinator of this group is Thomas Kutter (Louisiana State University) and the interim manager is Greg Pawloski (University of Minnesota). Coordinator responsibilities include defining operational requirements, communicating with the CERN SPSC and leaders of the CERN neutrino platform, as well as coordination of all activities associated with the installation, commissioning, and operation of the detector in the CERN test beam area. The design and construction of the DUNE-PT is undertaken by the DUNE Far Detector Organization, whose interim coordinator and manager is Jim Stewart (Brookhaven National Laboratory). The DUNE management team oversees all of the collaboration activities related to the design, construction, installation, commissioning, and operation of the

DUNE-PT through the collaboration Technical Board.

The DUNE Software & Computing and Physics Coordinators will form collaboration working groups focusing on simulation and data analysis efforts related to the CERN-PT. The current co-leaders of the DUNE effort to develop a comprehensive and prioritized list of measurements required to evaluate the performance of the detector and provide the particle response models necessary for DUNE sensitivity studies are Donna Naples (University of Pittsburgh) and Jaroslaw Nowak (University of Lancaster). Complementary efforts to define requirements on the test beam necessary for making these measurements and communicating with the CERN beamline coordinator on how to implement these requirements are headed by Cheng-Ju Lin (Lawrence Berkeley National Laboratory).

## 9.2 Schedule

The proposed schedule for constructing, installing, and operating the DUNE-PT is driven by the desire of the DUNE collaboration to complete these activities on a timescale that will inform construction of the the first 10 kt detector module at SURF, which has a scheduled installation beginning in early 2022. For this reason, the collaboration would ideally like to fully commission the detector and collect data for analysis prior to 2019. However, the primary collaboration goal of validating the design for the first 10 kt detector module at SURF can be mostly accomplished through the collection of cosmic ray data. Therefore, although it would be highly preferable to collect beam data prior to 2019, data collected after this date would still be available in time to play its essential role in understanding the data to be collected from the first 10 kt detector at SURF.

A schedule that allows for the collection of test beam data prior to 2019 is shown in Fig. 25. Detector construction is scheduled to begin in the second quarter of 2016 and the modules would be transported to CERN in two batches so that installation at the test beam site could begin as soon as the cryogenic infrastructure including the detector cryostat was available. Using this approach, the detector installation, which is expected to require a little under one year to complete, could be finished by the beginning of 2018, allowing for an early-2018 filling of the cryostat and a short data run prior to the shutdown. Detector construction times are informed by recent experience obtained from building prototype detector modules for the 35 t cryostat at Fermilab, which will start taking cosmic ray data in the fall of 2015.

## 9.3 Institutional Responsibilities

The deliverables required to construct and operate the DUNE-PT are summarized in Table 6. DUNE is a new collaboration recently organized to incorporate former members of the LBNE and LBNO collaborations and other interested members into a unified effort to perform the best possible measurements of neutrino oscillations, proton decay, and supernova neutrinos using large-scale, deep-underground liquid argon detectors. Institutional responsibilities for specific detector construction activities are still under development. In Table 6, DUNE institutions expected to contribute to the production of specific detector elements needed for the DUNE-PT are listed. It should be noted that the participation of some institutions on this list is dependent on the acceptance of recently-submitted or future funding requests from their supporting agencies. A high

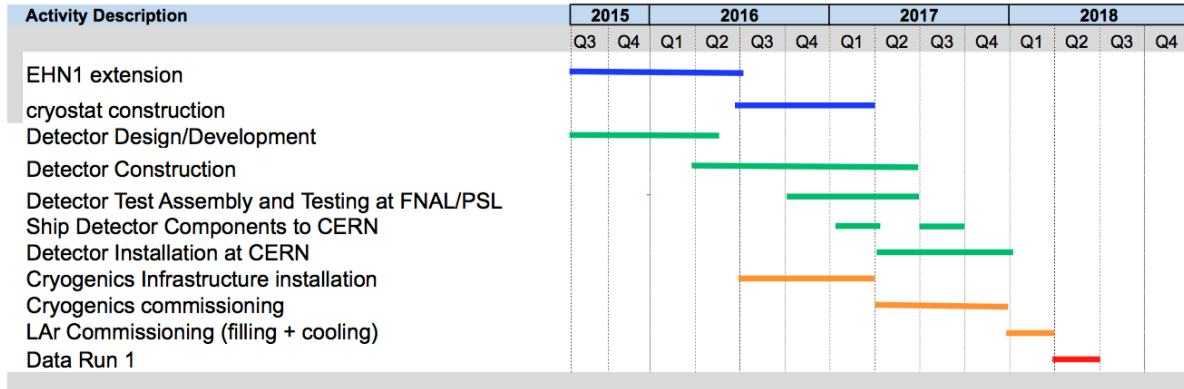


Figure 25: Rolled up version of a draft schedule for DUNE-PT. A 2 - 3 months data taking period is included in the schedule.

item no.	Deliverable	Contributing Institutes
1.	Single-phase LAr detector	
1.1	TPC	BNL, CERN, Lancaster, LBNL, Liverpool Manchester, Princeton, Sheffield, Wisconsin
1.2	Cold electronics	BNL, Fermilab, Penn, SMU
1.3	Photon detection system	ANL, Campinas, CSU, Hawaii, IU, LSU
1.4	DAQ	Cambridge, Duluth, Fermilab, LANL Oxford, SLAC
1.5	HV power supplies & feedthroughs	ETHZ, UCLA
1.6	Installation	CERN, Duke, Fermilab, Minnesota
1.7	Interfaces	BNL, LBNL, CERN, Fermilab
2.	Operation & Scientific Effort	
2.1	Operation	DUNE-PT collaborators
2.2	Software & Simulations	DUNE
2.3	Data analysis	DUNE

Table 6: List of work packages and deliverables for detector components and scientific effort.

priority for the DUNE collaboration management moving forward will be to finalize a matrix of responsibilities among the collaborating institutions. It is expected that this process will lead to a significant increase in the level of effort associated with the development of all required detector components. In the meantime, the institutions who have been involved in the proposed design of the DUNE-PT will be expected to push the effort forward during this transition period to ensure that the collaboration is able to maintain the proposed schedule for having detectors installed at CERN in early 2018.

Although the construction, installation, and operation of the DUNE-PT will be the responsibility of the DUNE collaboration, we do ask for support from the CERN neutrino platform in the form of detector infrastructure as summarized in Table 7. In particular, we ask for support for the construction and installation of the cryostat and supporting cryogenic systems needed to house and operate the experiment as well as access to common infrastructure within the CERN test beam area such as slow controls and data

item no.	Deliverable	Contributing Institutes
3.	Detector Infrastructure & Beam	
3.1	Cryostat	CERN
3.2	Cryogenics system	CERN
3.3	Infrastructure	CERN
3.4	Beam	CERN

Table 7: List of work packages and deliverables for infrastructure.

concatenation systems. We also request support from the CERN accelerator departments to provide the required beamline.

Construction, installation, and operation of the DUNE-PT will be conducted following all Fermilab and CERN safety regulations. DUNE management has direct line responsibility for safety and is assisted in this effort by the DUNE project ES&H manager, Mike Andrews (Fermilab).

## 9.4 Cost estimate and funding sources

Cost estimates in **core** accounting of the various detector components and infrastructure items that will be provided for the DUNE-PT by the participating members of the DUNE collaboration are shown in Table 8. Core M&S cost estimates do include the cost of the labor hours required to assemble and install the various detector components. Costing of the various detector components is informed by the previously mentioned construction activities associated with building prototype detectors for the 35 t cryostat at Fermilab.

Financial support for the construction and installation of the DUNE-PT will be obtained through the funding agencies of the various institutions involved in the effort. Current funding available for the effort is via the DUNE US project supported by the United States Department of Energy (DOE). It is expected that additional funding sources associated with non-DOE institutions will be obtained for this effort within the next year. However, even if this does not occur, the funding profile for the DUNE US project over the next three years is by itself sufficient for supporting DUNE responsibilities to the DUNE-PT, which the collaboration is supporting as its highest priority activity during this time period.

<b>Detector Element</b>	<b>core M&amp;S Cost [US \$]</b>	<b>core Labor [hours]</b>
Time Projection Chamber	1,210,000	6,200
Cold Electronics	1,260,000	4,500
Photon Detection System	610,000	4,200
DAQ	100,000	1,700
HV power supplies	300,000	300
Installation & Commissioning	30,000	12,400
Interfaces	110,000	2,500
<b>Totals</b>	<b>3,620,000</b>	<b>31,800</b>

Table 8: Estimated core costs and labor hours for the main DUNE-PT detector elements to be provided by the DUNE Collaboration

## 10 Summary

The single-phase detector design that is proposed in this document has been chosen as the reference design for the first 10 kt far detector module of the DUNE experiment. Although the single phase liquid argon technology has been successfully operated on a smaller scale, a liquid argon detector on the scale of the DUNE experiment has never been built before. In order to mitigate risks, DUNE-PT is a crucial milestone that will inform the construction and operation of the first 10 kt module for the DUNE far detector.

A goal of the DUNE-PT is to perform an engineering test to validate the mechanical and electrical performance of the full-scale detector components to inform decisions that need to be made well in advance of the 2022 installation date of the first 10 kt module. The primary goal of the DUNE-PT and beam test is to validate the physics performance of the detector in response to charged particles. It would be of great value to take charged particle beam data before the LHC long shutdown in 2018 to further inform strategic DUNE decisions. However, even beam data taken after the shutdown is instrumental in assessing systematic detector uncertainties for DUNE, validating and improving reconstruction algorithms for particle identification and energy reconstruction. A charged particle beam data set represents a golden detector calibration which improves DUNE’s sensitivity to its scientific goals. The DUNE experiment will have unprecedented sensitivity to CP violation in the lepton sector, the neutrino mass hierarchy, and certain proton decay modes.

The DUNE-PT represents the cumulation of years of R&D effort. The technology, data acquisition, computing, and installation procedures are mature and have been tested on smaller scales. There is a well established organization to implement the prototype program.

## References

- [1] "LBNF/DUNE Conceptual Design Report", <https://web.fnal.gov/project/LBNF/ReviewsAndAssessments/LBNF-DUNE%20CD-1-Refresh%20Directors%20Review/SitePages/Conceptual%20Design%20Report.aspx>
- [2] "Expression of Interest for a Full-Scale Detector Engineering Test and Test Beam Calibration of a Single-Phase LAr TPC" M.A. Leigui de Oliveira et al, SPSC-EOI-011, <http://cds.cern.ch/record/1953730/files/SPSC-EOI-011.pdf?version=1>
- [3] First scientific application of the membrane cryostat technology, D.Montanari et al, *AIP Proceedings 1573, 1664 (2014)* <http://scitation.aip.org/content/aip/proceeding/aipcp/10.1063/1.4860907>
- [4] Performance And Results of the LBNE 35 ton Membrane Cryostat Prototype *D.Montanari et al, 25th International Cryogenic Engineering Conference and the International Cryogenic Materials Conference in 2014, ICEC 25-ICMC 2014, LBNE Docid 9270*
- [5] I. De Bonis et al. (The LBNO-DEMO (WA105) Collaboration), Technical Design Report for large-scale neutrino detectors prototyping and phased performance assessment in view of a long-baseline oscillation experiment, CERN-SPSC-TDR-004, arXiv:1409.4405 (2014)
- [6] "The Liquid-argon time projection chamber: a new concept for Neutrino Detector", C. Rubbia, CERN-EP/77-08 (1977).
- [7] "Design, construction and tests of the ICARUS T600 detector", ICARUS Collaboration, Nucl. Inst. Meth., A527 (2004) 329-410. "Performance of a liquid argon time projection chamber exposed to the CERN West Area Neutrino Facility neutrino beam", F. Arneodo et al. (ICARUS-Milano Collaboration) - Physical Review D (2006) (Vol. 74, No. 112001).
- [8] "First Measurements of Inclusive Muon Neutrino Charged Current Differential Cross Sections on Argon." C. Anderson et al, Physical Review Letters (PRL) 108 (2012), 161802.
- [9] "The ArgoNeuT Detector in the NuMI Low-Energy beam line at Fermilab" C. Anderson et al, Journal of Instrumentation (JINST), 2012 JINST Vol. 7 P10019.
- [10] <http://intensityfrontier.fnal.gov/lariat.html>
- [11] H. Berns et al. [The CAPTAIN Collaboration], arXiv:1309.1740 [physics.ins-det].
- [12] "FLUKA: a multi-particle transport code" A. Ferrari, P.R. Sala, A. Fassio, and J. Ranft, CERN-2005-10 (2005), INFN/TC\_05/11, SLAC-R-773.
- [13] "Measurement of neutrino-induced charged-current charged pion production cross sections on mineral oil at  $E \sim 1$  GeV" A. A. Aguilar-Arevalo, et al., Phys. Rev. D 83, 052007 (2011).

- [14] "Charged Pion Production in Interactions on Hydrocarbon at  $\bar{E}= 4.0$  GeV", B. Eberly et. al., arXiv:1406.6415 [hep-ex].
- [15] "The GENIE Neutrino Monte Carlo Generator", C. Andreopoulos, et al., Nucl. Instrum. Meth. A614, 87 (2010).
- [16] "Pion-nucleus Interactions", T. S. H. Lee and R. P. Redwine, Ann. Rev. Nucl. Sci, **52**, 23 (2002).
- [17] "The columnar theory of ionization", Ann. Phys. **42**, 303 (1931).
- [18] "A study of electron recombination using highly ionizing particles in the ArgoNeuT Liquid Argon TPC", R. Acciarri et al, Journal of Instrumentation (JINST), 2013 JINST Vol. 8 P08005.
- [19] "Study of electron recombination in liquid argon with the ICARUS TPC", S. Amoruso et. al, NIM A **523**, 275 (2004).
- [20] "Neural Network Parameterizations of Electromagnetic Nucleon Form Factors", K. M. Graczyk, P. Plonski, R. Sulej, JHEP Vol. 2010, No 9, pp.1-30 (2010).
- [21] NetMaker, <http://www.ire.pw.edu.pl/~rsulej/NetMaker>
- [22] "Precise 3D track reconstruction algorithm for the ICARUS T600 liquid argon time projection chamber detector", ICARUS Collaboration, Adv.High Energy Phys., vol. 2013, p. 260820, 2013
- [23] "Experimental search for the LSND anomaly with the ICARUS detector in the CNGS neutrino beam", ICARUS Collaboration, Eur. Phys. J. C (2013) 73:2345.
- [24] "Results from and Status of ArgoNeuT and MicroBooNE" A. Szec., XXVI International Conference on Neutrino Physics and Astrophysics (<http://neutrino2014.bu.edu/>).
- [25] LBNE docdb #9079, <http://lbne2-docdb.fnal.gov/cgi-bin/ShowDocument?docid=9079>
- [26] "Nucleon Decay Searches with large Liquid Argon TPC Detectors at Shallow Depths: atmospheric neutrinos and cosmogenic backgrounds", A.Bueno, Z.Dai, Y.Ge, M.Laffranchi, A.J.Melgarejo, A.Meregaglia, S.Navas, A.Rubbia, JHEP 0704:041, (2007).
- [27] "A system to test the effects of materials on the electron drift lifetime in liquid argon and observations on the effect of water", R. Andrews, et al., Nucl. Instrum. Meth. A608 (2009) 251-258
- [28] LBNF/DUNE Conceptual Design Report Annex 4A: The LBNE Design for a Deep Underground Single-Phase Liquid Argon TPC," LBNE-doc-10685 <http://lbne2-docdb.fnal.gov/cgi-bin/ShowDocument?docid=10685>

- [29] LBNE docdb #6471, <http://lbne2-docdb.fnal.gov/cgi-bin/ShowDocument?docid=6471>
- [30] LBNE docdb #6140, <http://lbne2-docdb.fnal.gov/cgi-bin/ShowDocument?docid=6140>
- [31] E. Grace, J. Nikkel, arXiv: 1502.04213
- [32] B. Jones et al., arXiv: 1306.4605
- [33] E. Grace, J. Nikkel, arXiv: 1502.04213
- [34] B. Jones et al., arXiv: 1306.4605
- [35] SensL SiPM, <http://sensl.com/products/silicon-photomultipliers/cseries/>
- [36] <http://sbn-nd.fnal.gov/>
- [37] R. Rebel et al., *Journal of Physics: Conference Series* **308** (2011) 012023; doi:10.1088/1742-6596/308/1/012023
- [38] IceCube Data Movement, <https://icecube.wisc.edu/science/data/datamovement>.
- [39] "Data processing and storage in the Daya Bay Reactor Antineutrino Experiment" M. He, *Nucl. Phys. B Proceedings Supplement* 00 (2015) 1–5 (<http://arxiv.org/pdf/1501.06969.pdf>).
- [40] "Prompt reconstruction of LHC collision data with the ATLAS reconstruction software" N.Barlow et al, *Journal of Physics: Conference Series* 331 (2011) 032004
- [41] LBNE doc-db #6547; <http://lbne2-docdb.fnal.gov/cgi-bin/ShowDocument?docid=6547>

# Appendix

## Cryostat

**Design parameters:** The design parameters for the CERN prototype cryostat are listed in Table 9.

**Insulation system and secondary membrane:** The membrane cryostat requires insulation applied to all internal surfaces of the outer support structure and roof in order to control the heat ingress and hence required refrigeration heat load. To avoid bubbling of the liquid argon inside the tank, the maximum static heat leak is  $10 \text{ W/m}^2$  for the floor and the sides and  $15 \text{ W/m}^2$  for the roof, higher to account for the penetrations that increase the heat budget. Preliminary calculations show that these values can be obtained using 0.9 m thick insulation panels of polyurethane foam. Given an average thermal conductivity coefficient for the insulation material of  $0.0283 \text{ W/(m}\cdot\text{K)}$ , the heat input from the surrounding steel is expected to be about 3.2 kW total. It assumes that the hatches are foam insulated as well. This is shown in Table 10.

**Top cap:** Table 11 presents the list of the design parameters for the top of the cryostat.

<b>Design Parameter</b>	<b>Value</b>
Type of structure	Membrane cryostat
Membrane material	SS 304/304L, 316/316L or equivalent.
Fluid	Liquid argon (LAr)
Other materials upon approval.	
Outside reinforcement (support structure)	Steel enclosure with metal liner to isolate the outside from the insulation space, standing on legs to allow for air circulation underneath.
Total cryostat volume	538 m <sup>3</sup>
Total LAr volume	483 m <sup>3</sup>
LAr total mass	673,000 kg
Minimum inner dimensions (flat plate to flat plate).	7.8 m (W) x 8.9 m (L) x 8.1 0 (H)
Depth of LAr	7.2 m (0.82 m ullage, same as LBNF)
Primary membrane	1.2 mm thick SS 304L corrugated stainless steel
Secondary barrier system	GTT design; 0.07 mm thick aluminum between fiberglass cloth. Overall thickness 1 mm located between insulation layers.
Insulation	Polyurethane foam (0.9 m thick from preliminary calculations)
Maximum static heat leak	10 W/m <sup>2</sup>
LAr temperature	88 +/- 1K
Operating gas pressure	Positive pressure. Nominally 70 mbarg (~1 psig)
Vacuum	No vacuum
Design pressure	350 mbarg (~5 psig) + LAr head (1,025 mbarg)
Design temperature	77 K (liquid nitrogen temperature for flexibility)
Temperature of all surfaces in the ullage during operation	<100 K
Leak tightness	10 <sup>-6</sup> mbar*1/sec
Maximum noise/vibration/microphonics inside the cryostat	LAr pump outside the cryostat
Beam window	Precise location TBD. Multiple beam windows installed on the upstream side of the cryostat
Accessibility after operations	Capability to empty the cryostat in 30 days and access it in 60 days after the end of operations.
Lifetime / Thermal cycles	Consistent with liquid argon program. TBD.

Table 9: Design requirements for the membrane cryostat

<b>Element</b>	<b>Area (<math>m^2</math>)</b>	<b>K (<math>W/mK</math>)</b>	<b><math>\Delta T</math> (<math>K</math>)</b>	<b>Heat Input (<math>W</math>)</b>
Base	83	0.0283	205	534
End walls	153	0.0283	205	986
Side walls	172	0.0283	205	1,108
Roof	83	0.0283	205	550
Total				3,162

Table 10: Heat load calculation for the membrane cryostat (insulation thickness=0.9 m).

Design Parameter	Value
Configuration	Removable metal plate reinforced with trusses/I-beams anchored to the membrane cryostat support structure. Contains multiple penetrations of various sizes and a manhole. Number, location and size of the penetrations TBD. The hatches shall be designed to be removable. If welded, provisions shall be made to allow for removal and re-welding six (6) times.
Plate/Trusses non-wet material	Steel if room temperature. SS 304/304 or equivalent if at cryogenic temperature
Wet material	SS 304/304L, 316/316L or equivalent. Other materials upon approval.
Fluid	Liquid argon (LAr)
Design pressure	350 mbarg ( 5 psig)
Design temperature	77 K (liquid nitrogen temperature for flexibility)
Inner dimensions	To match the cryostat
Maximum allowable roof deflection	0.003 m (differential between APA and CPA)
Maximum static heat leak	<15 W/m <sup>2</sup>
Temperatures of all surfaces in the ullage during operation	<100 K
Additional design loads	<ul style="list-style-type: none"> <li>- Top self-weight</li> <li>- Live load (488 kg/m<sup>2</sup>)</li> <li>- Electronics racks (400 kg in the vicinity of the feed through)</li> <li>- Services (150 kg on every feed through)</li> </ul>
TPC anchors	Number and location TBD. Minimum 6.
Hatch opening for TPCs installation	3.550 m x 2.000 m (location TBD)
Grounding plate	1.6 mm thick copper sheet brazed to the bottom of the top plate
Lifting fixtures	Appropriate for positioning the top at the different parts that constitute it.
Penetrations	<ul style="list-style-type: none"> <li>1 LAr In, 1 Purge GAr In, 1 Vent GAr In</li> <li>2 Pressure Safety Valves, 2 Vacuum Safety Valves</li> <li>1 GAr boil off to condenser</li> <li>1-2 Liquid level sensors</li> <li>1-2 Instrumentation</li> <li>1 Temperature sensors feedthroughs?</li> <li>1 LAr for cool down, 1 GAr for cool down</li> <li>1 TPC signal, 3 TPC feedthroughs</li> <li>1 Photon Detector for APA (Cold)</li> <li>Calibration dc</li> </ul>
Lifetime / Thermal cycles	Consistent with the liquid argon program TBD.

Table 11: Design parameters for the top of the cryostat